universität wien

MASTERARBEIT / MASTER'S THESIS

Titel der Masterarbeit / Title of the Master's Thesis

Development of a commissioning tool for the independent dose calculation software IDEAL for the patient specific quality assurance at MedAustron

verfasst von / submitted by

Lukas Scheuchenpflug, BSc

angestrebter akademischer Grad / in partial fulfilment of the requirements for the degree of

Master of Science (MSc)

Wien, 2020 / Vienna, 2020

Studienkennzahl lt. Studienblatt / degree programme code as it appears on the student record sheet:	A 066 876
Studienrichtung lt. Studienblatt / degree programme as it appears on the student record sheet:	Physics / Physik
Betreut von / Supervisor:	Univ.-Prof. Dipl.Ing. Dr. Robin Golser

Abstract

Introduction: At MedAustron, every treatment plan is dosimetrically verified before the first treatment using 24 pin-point ionization chambers. This process is called measurement-based Patient Specific Quality Assurance (PSQA). A Monte Carlo-based independent dose calculation tool called IDEAL (based on GATE-RTion1.0 and GEANT4 10.03p3) will partly replace the current PSQA process. This work describes the development of a commissioning tool for IDEAL as well as a first application. This tool, called ReadOutScript (ROS), has been developed for the fixed horizontal beam line and follows the IEC 62304 standard. It has been implemented and tested using proton dose distributions.

Material and Methods: The ROS reads a 3D DICOM-DOSE file and evaluates it against a set of 24 ionization chamber measurements. Treatment plans of different scoring resolutions produced with the Treatment Planning System (TPS) RayStation (RSv5.99, RSL) were used in order to validate the ROS. Another TPS-dedicated and validated script used for similar purposes was used as reference to validate the ROS. Since this script is implemented in the TPS, it cannot be used for the commissioning of IDEAL. As a first application, the ROS has been used to evaluate a version of IDEAL (v0.9). A total of 47 IDEAL-generated proton dose distributions were evaluated against measurement for homogeneous cubic dose distributions, irregular targets, plans at Isocenter (ISD0cm) and at an Isocenter to phantom Surface Distance of 50 cm (ISD50cm) as well as plans with and without range shifter.

Results: Evaluating the extraction of the ROS against the already validated TPS-implemented script resulted in a mean global signed $\langle \Delta D \rangle$ and unsigned dose difference $\langle \Delta D_{ABS} \rangle$ of -0.05 % and 0.15 %, respectively. A first evaluation of IDEALv0.9-generated plans show an agreement of ($\langle \Delta D \rangle = 0.5\,\%$, $\langle \Delta D_{ABS} \rangle = 1.1\,\%$).

Discussion and Conclusion: The validation of the ROS has been successful and it can be used for commissioning. An evaluation of IDEALv0.9-generated plans (protons) show overall good agreement. Slightly better agreement was achieved for homogeneous cubic dose distributions, plans at ISD50cm and plans without range shifter.[1]

[1] A similar abstract was submitted to the "ÖGRO Jahrestagung 2019", Wiener Neustadt

Zusammenfassung

Einführung: Am MedAustron wird jeder Bestrahlungsplan vor der ersten Behandlung mit Hilfe von 24 Ionisationskammern dosimetrisch verifiziert. Eine, auf der Monte Carlo-Methode basierende, unabhängige Dosisberechnungssoftware namens IDEAL (basierend auf GATE-RTion1.0 und GEANT4 10.03p3) wird dazu verwendet werden, die gegenwärtige patientenspezifische Qualitätssicherung teilweise abzulösen. Diese Masterarbeit beschreibt die Entwicklung und erste Anwendung einer Software, welche später für die Kommissionierung von IDEAL herangezogen wird. Diese Kommissionierungssoftware trägt den Namen ReadOutScript (ROS) und wurde gemäß dem IEC 62304 Standard entwickelt. Sie wurde unter Verwendung von Protonen Dosisverteilungen für die horizontale Strahllinie am MedAustron implementiert und gestestet.

Methodik: Das ROS liest eine IDEAL-generierte dreidimensionale Dosisverteilung und eine Reihe an Messungen der 24 Ionisationskammern und wertet diese aus. Um das ROS zu validieren wurden Bestrahlungspläne verschiedener Auflösung, welche mit der Software TPS RayStation (RSv5.99, RSL) erstellt wurden, verwendet. Ein bereits validiertes Programm, welches in der MedAustron Bestrahlungsplanungssoftware (TPS) integriert ist, wurde als Referenz für die Validierung des ROS herangezogen. Dieses Programm selbst darf nicht für die Kommissionierung von IDEAL eingesetzt werden, um die Unabhängigkeit des Kommissionierungsprozesses zu gewährleisten. Eine Auswertung der aktuellen Version von IDEAL (v0.9) stellte die erste Anwendungsmöglichkeit für das ROS dar. Insgesamt wurden 47 Dosisverteilungen (Protonen) mit IDEAL erzeugt und mit Messungen verglichen, darunter homogene und irreguläre Dosisverteilungen, Pläne mit ISD50cm (Isocenter to phantom Surface Distance of 50 cm) und ISD0cm und Pläne mit und ohne range shifter.

Resultate: Ein Vergleich mit der bereits validierten und TPS-implementierten Software ergab eine mittlere globale Dosisdifferenz $\langle \Delta D \rangle$ von $-0,05\,\%$ und eine absolute mittlere globale Dosisdifferenz $\langle \Delta D_{ABS} \rangle$ von $0,15\,\%$. Eine erste Auswertung der IDEALv0.9-generierten Pläne zeigt eine Übereinstimmung von ($\langle \Delta D \rangle = 0,5\,\%$, $\langle \Delta D_{ABS} \rangle = 1,1\,\%$) auf.

Diskussion: Das ROS wurde erfolgreich validiert und darf für die Kommissionierung verwendet werden. Die Auswertung der IDEALv0.9-generierten Pläne stimmt insgesamt gut mit den Messungen überein. Homogene Dosisverteilungen und Pläne mit ISD50cm und Pläne ohne range shifter zeigen tendenziell eine bessere Übereinstimmung auf.

Preface

From April to October of 2019 I have been working on this project at MedAustron in Wiener Neustadt in the department Medical Physics, specifically in the group Monte Carlo and Beam Delivery. This thesis reports on this project. A special thanks goes to Loïc Grevillot, who was my direct advisor at MedAustron and who is leading this project. Another thanks goes to Markus Stock, head of Medical Physics at MedAustron, who has given me this opportunity. Both of whom have done me a great favor by reviewing this thesis. On top of that I want to thank Robin Golser, group speaker Isotope Physics, University of Vienna, who was kind enough to accept advisor-ship of my thesis.

I would also like to mention David J. Boersma, who has developed IDEAL; Rubén Gleyzes Gonzalo, who has developed the 1D and 2D commissioning tools of TEDD as well as the majority of the GUI of TEDD; Hermann Fuchs, who has provided me with a python tool for dose extraction, which served as a first inspiration for the development of TEDD 3D (ROS) and lastly, Till Böhlen, who has developed the "AnalysisPinPoint.py"-script, which was used for producing a majority of the plots in this thesis.

Contents

Abbreviations

DDS	Dose Delivery System
GATE	Geant4 Application for Emission Tomography
GEANT4	GEometry ANd Tracking 4
HRP	Holder Reference Point
IC	Ionization Chamber
IDC	Independent Dose Calculation
IS	Inferior-Superior
ISD	Isocenter to phantom Surface Distance
IDEAL	Independent DosE CalculAtion system for Light ion beam radiotherapy
ITS	Independent Termination System
MC	Monte Carlo
MCS	Multiple Coulomb Scattering
NS	Nuclear Scattering
PA	Posterior-Anterior
PBA	Pencil Beam Algorithm
PSQA	Patient Specific Quality Assurance
PP	Pin-Point
RaShi	Range Shifter
RFQ	Radio Frequency Quadrupole
RiFi	Ripple Filter
ROS	Read Out Script
SOBP	Spread Out Bragg Peak
TEDD	Toolkit for Evaluation of DICOM Doses
TPS	Treatment Planning System

1 Introduction

1.1 The burden of cancer

According to Bray et al. (2018), who comprised GLOBOCAN data, the worldwide burden of cancer was estimated at 9.5 million deaths and 17 million new cases (excl. non-melanoma skin cancer) in 2018. Lung cancer poses the highest rate of cancer deaths, followed by female breast cancer and prostate cancer. A more detailed breakdown of incidences and deaths by cancer type can be seen in figure 1. In 91 out of 172 countries cancer is the highest or second highest ranking cause of premature death and it is likely to be the number one cause of death globally in the 21st century (Bray et al., 2018, p. 394).

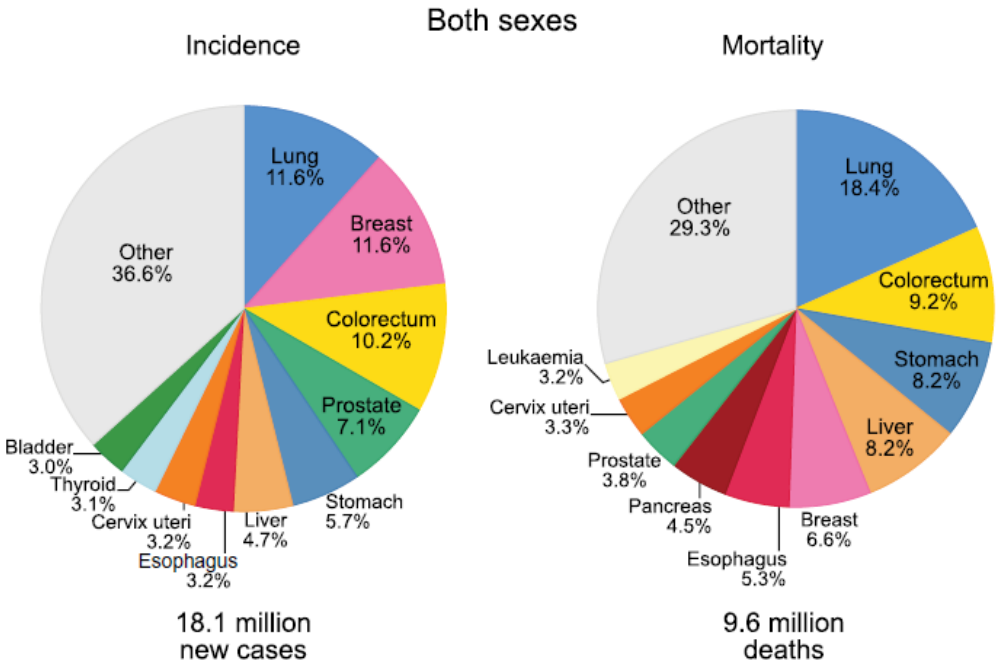

Figure 1: 10 most frequent cancer incidences and deaths world wide with data from GLOBOCAN 2018 (Bray et al., 2018, p. 400)

1.2 Cancer treatment

There are generally three types of cancer treatment: Surgical removal, systemic therapy and radiotherapy. Radiotherapy can be either external or internal (brachytherapy). The latter refers to the insertion of radioactive material directly into the tumor. External radiotherapy refers to the usage of beams of ionizing radiation that penetrate the patient. This is done most commonly by the means of photons or electrons sometimes referred to as conventional radiotherapy (Sánchez Parcerisa, 2012, p. 2). Radiotherapy is often used alongside surgery or chemotherapy. Out of the approximately 45 % of patients diagnosed with cancer that can be successfully cured,

23 % are treated radio-therapeutically. Approximately 5 % in combination with chemotherapy, 6 % in combination with surgery and 12 % exclusively with radiotherapy (IAEA, 2008, p. 1).

1.3 The physics of proton beam therapy

The treatment with protons was first suggested by Wilson (1946) and first attempted at the Lawrence Berkeley National Laboratory (Tobias et al., 1958).

Charged particles, such as protons, show a dose distribution, which sharply peaks over the last several millimeters of their range (Bragg-Peak). This behavior can be exploited for treatment applications by reducing the exposure to healthy tissue. The penetration depth of the charged particles can be adjusted by varying the initial energy. In tumor treatment, multiple fields of different energies can be used consecutively to allow for a conformal dose distribution matching the tumor (Levin et al., 2005, pp. 849-850). This can be seen in figure 2.

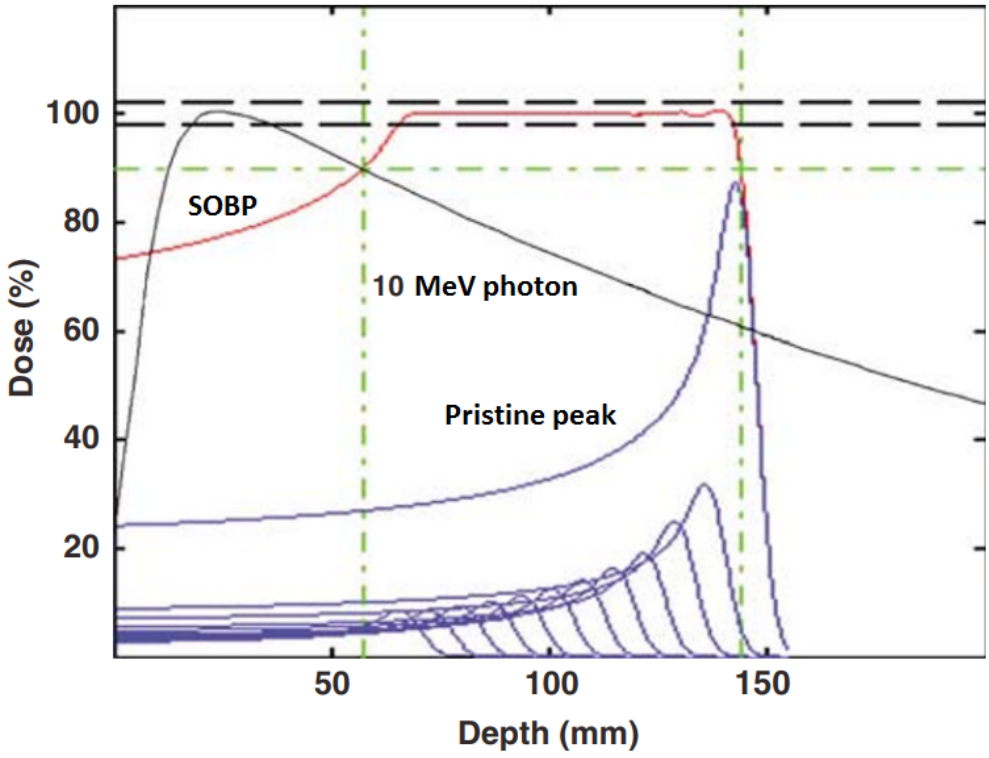

Figure 2: The composition of several Bragg curves of descending initial energies, starting with the pristine Bragg-Peak (blue), results in a Spread-Out Bragg-Peak (red). The dose distribution of a 10 MeV photon beam shown for comparison (black). Image adapted from (Levin et al., 2005, p. 850) This pristine Bragg-Peak would correspond to an energy of roughly 150 MeV for protons in water

The most relevant processes by which protons interact with matter are listed in figure 1. Protons experience a continuous energy loss due to coulomb interactions with electrons in the target material. These result in little directional change due to the large mass of protons com-

Interaction type	Interaction target	Principal ejectiles	Influence on projectile	Dosimetric manifestation
Inelastic Coulomb scattering	Atomic electrons	Primary proton, ionization electrons	Quasi-continuous energy loss	Energy loss determines range in patient
Elastic Coulomb scattering	Atomic nucleus	Primary proton, recoil nucleus	Change in trajectory	Determines lateral penumbral sharpness
Non-elastic nuclear reactions	Atomic nucleus	Secondary protons and heavier ions, neutrons, and gamma rays	Removal of primary proton from beam	Primary fluence, generation of stray neutrons, generation of prompt gammas for *in vivo* interrogation
Bremsstrahlung	Atomic nucleus	Primary proton, Bremsstrahlung photon	Energy loss, change in trajectory	Negligible

Table 1: Types of interactions of protons traversing matter (Newhauser and Zhang, 2015, p. 159)

pared to electrons. Elastic collisions with nuclei of the target material, however, deflect primary protons. In the case of multiple coulomb scattering, the net scattering angle can be approximated statistically. Non elastic collisions with target nuclei can lead to secondary particles such as neutrons, protons, deuterium or heavier ions. The contribution of Bremsstrahlung is negligible for radio-therapeutic energies (Newhauser and Zhang, 2015, pp. 158-170).

The mass stopping power of a beam is defined as the linear stopping power (energy loss per unit distance) over the density of the target material ($-\frac{dE}{\rho dx}$). A quantum-mechanical and relativistic description of the mass stopping power is given by the Bethe-Bloch equation (Newhauser and Zhang, 2015, p. 159):

$$-\frac{dE}{\rho dx} = 4\pi N_A r_e^2 m_e c^2 \frac{Z}{A}\frac{z^2}{\beta^2}\left[\ln\frac{2m_e c^2\gamma^2\beta^2}{I} - \beta^2 - \frac{\delta}{2} - \frac{C}{Z}\right] \tag{1}$$

ρ	density target material	Z	atomic number target material
N_A	Avogadro's constant	A	atomic weight target material
r_e	classical electron radius	I	mean excitation potential target material
m_e	electron mass	δ	density correction
z	atomic number projectile	C	shell correction

Table 2: Explanation of terms in Bethe-Bloch equation. γ, β, c have their common definitions. (Newhauser and Zhang, 2015, p. 159)

It is worth noting that there is no dependency on the mass of the primaries. The properties of the primary particles that do factor into the equation are its charge (z^2) and velocity $(\frac{1}{\beta^2})$. In terms of the target material, the linear stopping power is determined by the electron density $(N_A \rho \frac{Z}{A})$ and the mean excitation energy I. The electron density represents the dominant term, considering the logarithmic dependency on I. At high energies the energy loss declines due to the shielding of remote electrons by more proximate electrons, which is taken into account by the density correction δ. At energies low enough for the velocity of primary protons to be in the vicinity of the shell electrons of the target material, the shell correction term C takes effect (Newhauser and Zhang, 2015, p. 159).

1.4 MedAustron

The MedAustron light ion beam therapy centre in Wiener Neustadt (Austria) began first patient treatment on the 14^{th} of December 2016. It is a dual-particle facility, using both carbon ions and protons for treatment. That is why a synchrotron design has been chosen. A top view of the facility can be seen in figure 3. The clinical energies for protons range form 62.4 MeV to 252.7 MeV, which corresponds to a penetration depth of 3 cm to 38 cm in water. However, the accelerator has the capacity of producing protons up to 800 MeV for non-clinical research purposes. A maximum field size of 20 $\times$ 20 cm at isocenter can be achieved. The intensity of the beam can be reduced (by 50 %, 80 % and 90 %) by introducing a degrader in the beam path before the particles enter the synchrotron. In general, the accelerator can be split in three parts, the injector, the synchrotron and the transport lines (Schreiner et al., 2019, pp. 22-23).

A low-energy beam transport system guides the ions from one of three ion sources into the linear accelerator (LINAC). A radio frequency quadrupole accelerates the particles at first to 400 keV/u and an Inter Digital H-mode (IH) drift-tube LINAC accelerates them to an energy of 7 MeV/u before injection to the synchrotron ring. The particles pass a thin carbon foil, which serves as an electron stripper, before entering the synchrotron (Osmić et al., 2014, p. 2146).
In the case of proton treatments, H_+^3-ions are produced in the ion source, which are then fragmented into three protons and fully ionized at the electron stripper (Jägerhofer and Wurzer, 2017, p. 362). The injector can be seen in figure 4.

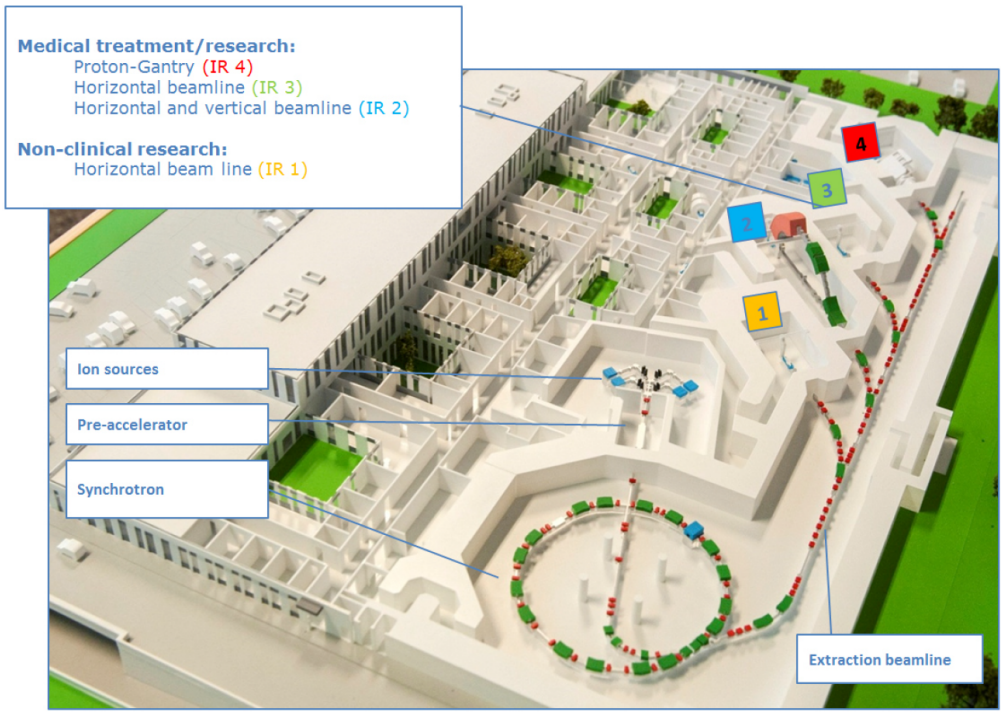

Figure 3: Top view of MedAustron showing the accelerator and irradiation rooms. Image from Stock et al. (2015)

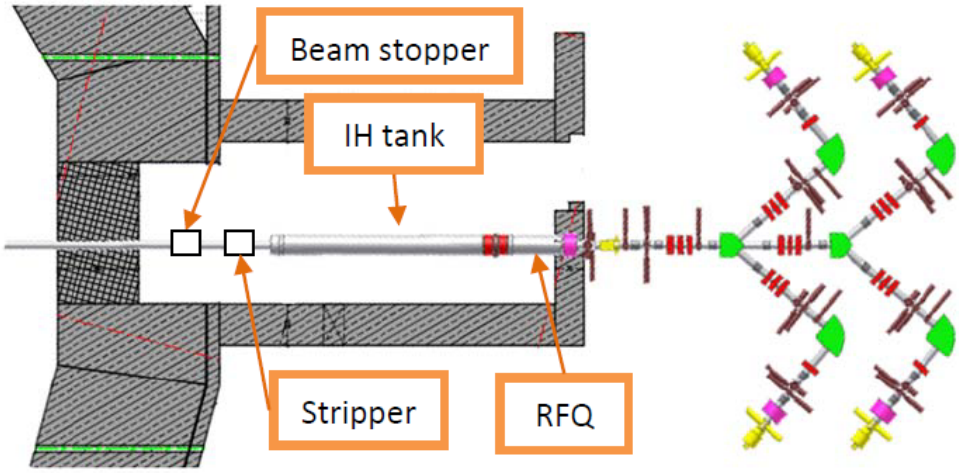

Figure 4: Low energy transfer line and four ion sources on the right. LINAC-bunker on the left. Image from (Benedikt et al., 2010, p. 110)

The particles are injected into the synchrotron in a multi-turn method and accelerated by a radio frequency cavity to the clinically required energy. The particles are extracted (slow extraction) and guided to one of the Irradiation Rooms (IRs). The maximum number of protons per spill is 2×10^{10} and the spill length ranges from $1\,s$ to $10\,s$. The approximately $400\,m$ long vacuum pipes of the transport line are kept at a pressure of $5 \times 10^{-9}\,mbar$ (Carlino, 2017, pp. 40-41). IR1 employs a horizontal beam-line and is dedicated for non-clinical research. IR3 employs a horizontal and IR2 a horizontal and vertical beam-line and IR4 contains a proton gantry based

on the gantry used at the Paul Scherrer Institute in Switzerland. The design of the accelerator was developed in collaboration with CERN (Geneva, Swizerland) and the National Center for Oncological Hadrontherapy (Pavia, Italy) (Carlino, 2017, p. 37).

The MedAustron beam delivery utilizes a "quasi-discrete spot scanning technique". (Carlino, 2017, p. 32). A tumor is virtually dissected into layers of the same radiological depth. A mono-energetic pencil beam is magnetically steered in X- and Y-direction to cover the entire layer at given depth laterally (ICRU, 2016, p. 41). During this process the beam is not shut off. The particle fluence is measured and the beam is moved to the next voxel once the required number of particles is reached. Once all voxels of a given slice are covered, the particle energy is reduced by the accelerator and the next layer is treated (Carlino, 2017, p. 32). A schematic of a nozzle can be seen in figure 5. The spot size ranges from approximately 7 mm at 252.7 MeV to about 22 mm at 62.4 MeV at isocenter (Carlino, 2018b, p. 6).

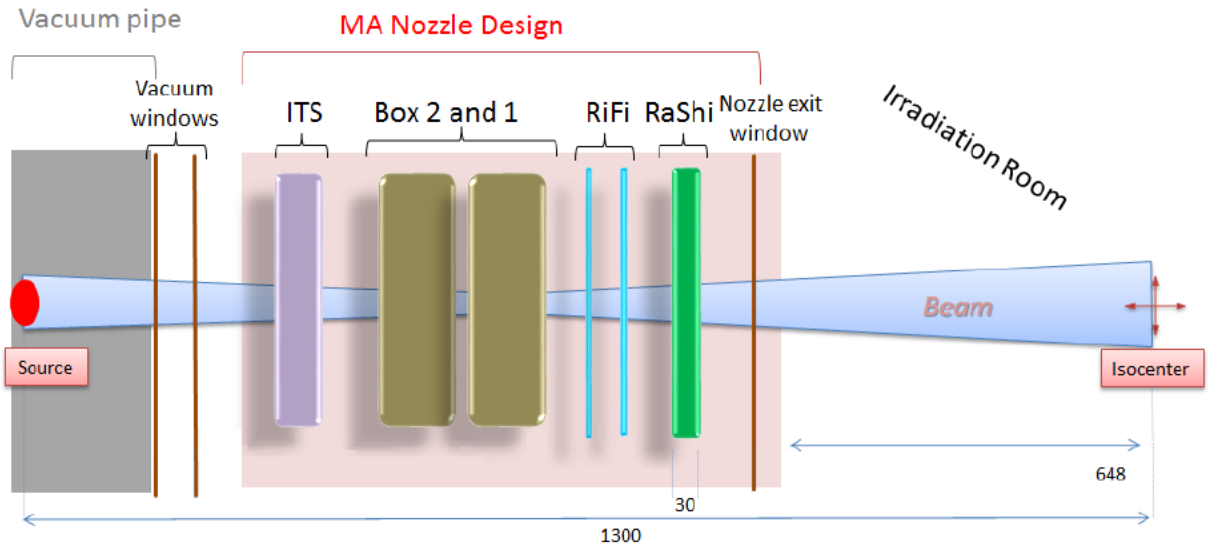

Figure 5: Nozzle at MedAustron. (Components from left to right) double foil vacuum window, Independent Termination System (ITS), Dose Delivery System (DDS) made up of Box 1 and 2, Ripple Filters (RiFis), Range Shifter (RaShi). Image from (Elia, 2019, p. 37)

The design of the nozzle is the same for all fixed beam lines and is functional both for protons and carbon ions. Each of the two boxes that make up the DDS consist of an integral chamber to measure the number of ions delivered to a given spot and of two perpendicular strip ionization chambers that measure both the position and the size of the beam. The ITS contains an integral chamber and terminates the beam if required. It is a redundant, independent safety system should the DDS not detect a malfunction. (Grevillot et al., 2019, p. 383) The ripple filters can

be used to modulate the width of the Bragg Peak if needed. This is generally not necessary for protons, although it can be used, but it is of importance for carbon ion treatments. The range shifter is used for targets at shallow depths (Elia, 2019, p. 37).

A distinguishing feature of MedAustron is the use of non-isocentric scanned proton and carbon treatments. The air gap between the patient and the nozzle is reduced by moving the patient closer to the exit window of the nozzle and therefore minimizing a spreading of the beam laterally. This is commonly used when a range shifter[2] is employed during treatment, which introduces a source of scattering and therefore increases the width of the beam. The use of non-isocentric treatments, however, is not limited to the treatment with a range shifter. A standard position used for measurements at non-isocentricity is the ISocenter to phantom surface Distance of 50 cm (ISD50) (Grevillot et al., 2019, pp. 381-382).

1.5 PSQA at MedAustron

In light ion beam therapy, certain protocols are employed to ensure the accuracy of the dose prediction of the Treatment Planning System (TPS) as well as the proper functionality of the beam delivery system. This typically includes the experimental verification of every beam delivered to a patient. This process is referred to as Patient Specific Quality Assurance (PSQA) and is of utmost importance for proton and carbon treatments. If the measured and predicted doses are within clinical tolerances, the treatment plan can be used for treatment. Which measurement technique is used in the PSQA process differs from facility to facility. Among the most common are 2D ion chamber array detectors, film measurements and water phantoms equipped with pin-point ionization chambers (PPs). At MedAustron the latter technique is used (Elia, 2019, pp. 67-68).

First a clinical treatment plan is produced by a medical physicist with the TPS. After the plan is approved by the responsible radio-oncologist, the treatment plan goes into the PSQA process. This starts with the clinical treatment plan being recomputed for a water phantom, meaning all the machine parameters of the clinical plan are used and the dose distribution in water is calculated in the TPS (Figure 6). Such machine parameters include the number of layers, number of spots, the spot spacing, the energy layer and the spot weight. A TPS-dedicated MedAustron-developed python tool (MA_QA_v4.py) is used to determine the dose at 24 positions within this treatment plan. These 24 doses then have to be verified experimentally. The 24 doses

[2] A range shifter is a plate of attenuation material (PMMA), which can be inserted in the beam-path to reduce the range of the incident particles to shallow depths (Matysiak et al., 2016, p 391)

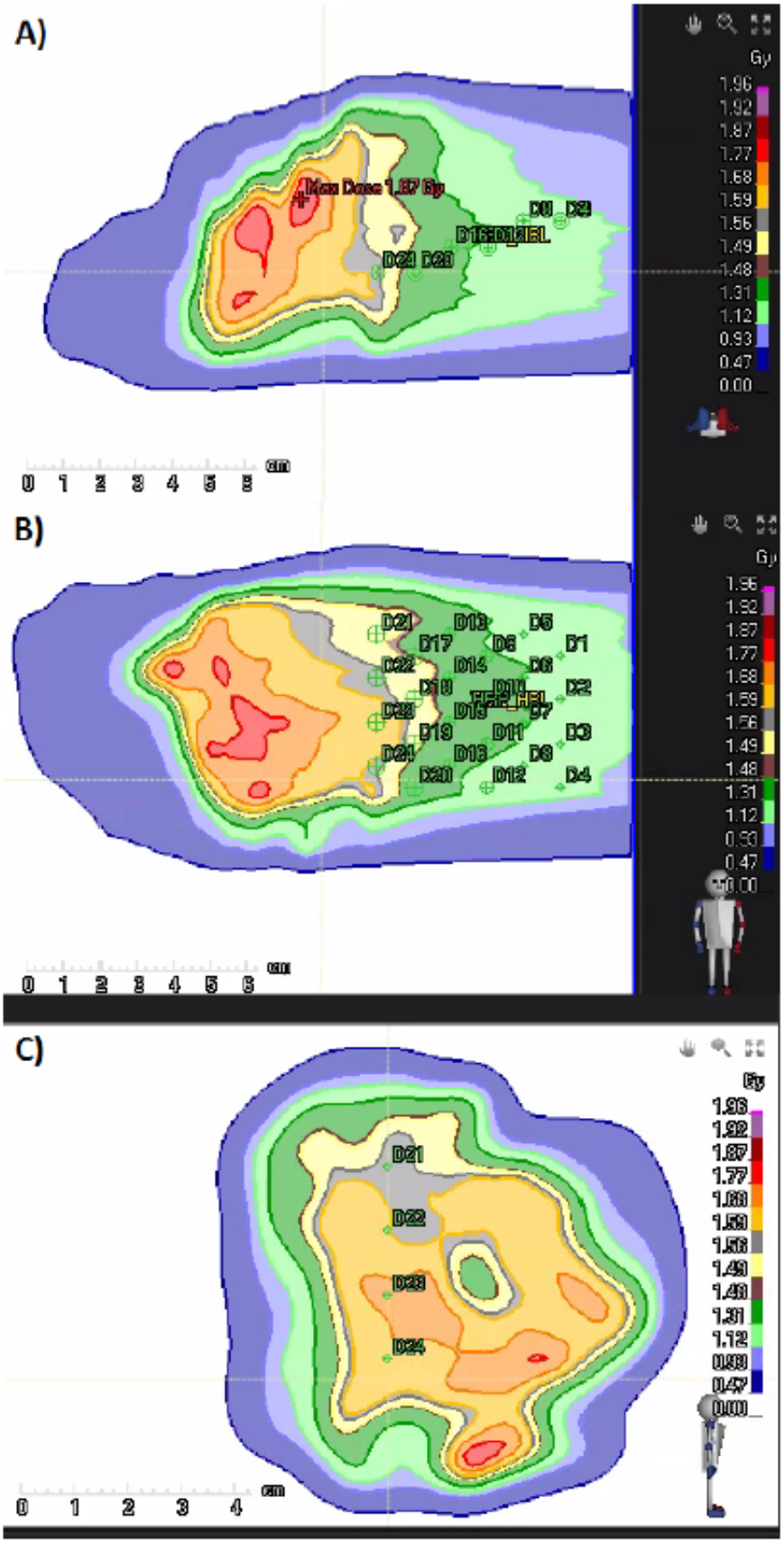

Figure 6: TPS-calculated dose distribution with 24 PPs in the transversal (A), coronal (B) and sagittal (C) view. Image from (Elia, 2019, p. 70)

and their location within the distribution are exported to a MedAustron-dedicated software called PlanVerificator, this represents the interface between the experimental tools and the TPS (Elia, 2019, p. 69).

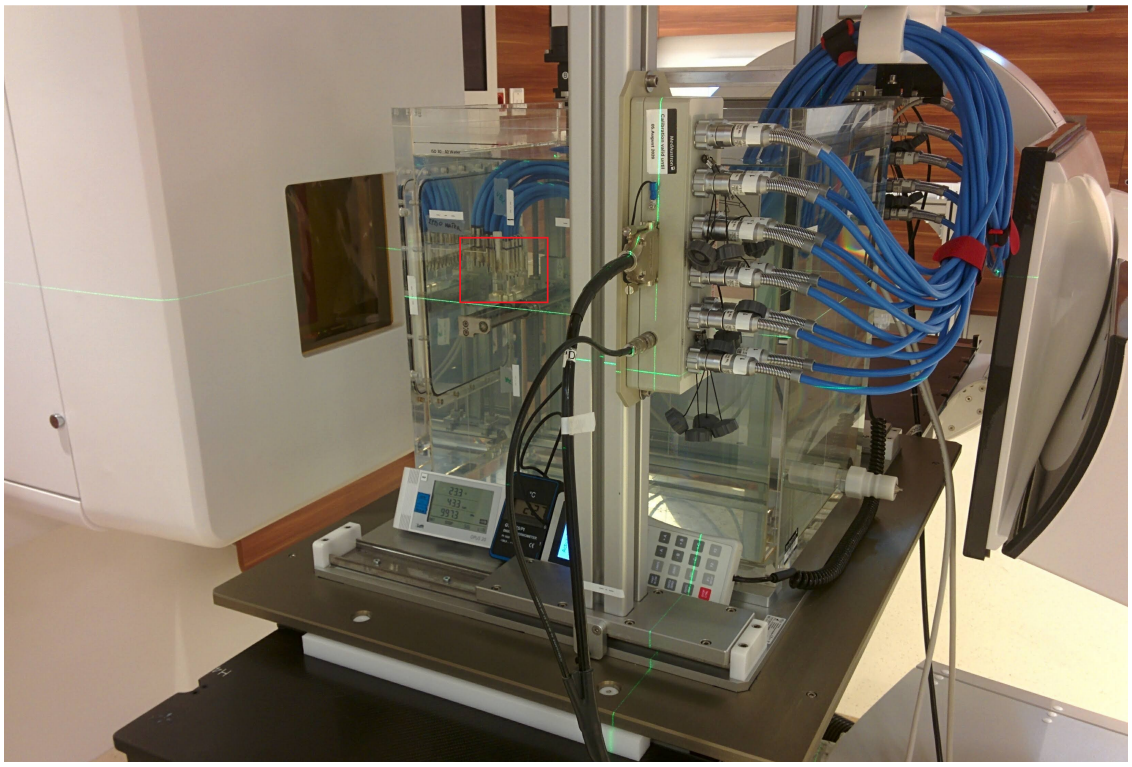

Figure 7: PSQA set-up. MP3-P water phantom mounted on treatment table placed downstream of the nozzle. The 3D-Block containing the 24 PPs is marked in red

The experimental setup can be seen in figure 7. The water phantom MP3-P (PTW, Freiburg) is mounted on the robotic treatment table ("couch"). A camera on the floor as well as a laser system facilitate the alignment process. To measure the dose, 24 pin-point ionization chambers are used (see figure 8). A schematic of one of the ionization chambers (ICs) can be seen in figure 9. The ICs are connected to two PTW-10004 MULTIDOS 12-channel electrometers, which provide a fixed high voltage supply of $+400\,V$. The 3D-Block is aligned with the laser system. The moving mechanism that positions the 3D Block containing the ICs within the water phantom has a resolution of 0.1 mm in all spatial dimensions (Elia, 2019, p. 69).
Once the experimental setup is finalized the phantom is irradiated and the dose measured. The 3D Block is moved to a specific position for each beam. The measured doses are then evaluated against the computed doses. At this point several definitions have to be introduced:

Dose difference (evaluated for each PP)

$$\Delta D^i = D^i_{meas} - D^i_{comp} \tag{2}$$

Local dose difference (evaluated for each PP)

$$\Delta D^i_{local} = \frac{D^i_{meas} - D^i_{comp}}{D_{comp}}\% \tag{3}$$

Global dose difference (evaluated for each PP)

$$\Delta D^i_{global} = \frac{D^i_{meas} - D^i_{comp}}{D_{max}}\% \tag{4}$$

Mean signed global dose difference (evaluated for each beam)

$$\langle \Delta D \rangle_{global} = \frac{1}{N}\sum_{i=1}^{N} \frac{D^i_{meas} - D^i_{comp}}{D_{max}}\% \tag{5}$$

Mean unsigned global dose difference (evaluated for each beam)

$$\langle \Delta D_{ABS} \rangle_{global} = \frac{1}{N}\sum_{i=1}^{N} \frac{|D^i_{meas} - D^i_{comp}|}{D_{max}}\% \tag{6}$$

where D_{meas}, D_{comp} and D_{max} are the measured, computed and maximum dose within the distribution, respectively. The index i corresponds to the individual ICs. N represents all ICs below the gradient-threshold. PPs showing a gradient (computed) larger than 0.04 Gy/mm are disregarded as a minimal positional offset during measurement results in a large dose difference. A variation of up to 7 % is tolerated for a single PP (Elia, 2019, p 72).

$$\Delta D^i_{global} \leq 7\% \tag{7}$$

The clinical acceptance criteria on the mean of the global signed and unsigned dose difference are as follows:

$$\langle \Delta D \rangle_{global} \pm \sigma(\langle \Delta D \rangle) \leq 5\% \pm 5\% \tag{8}$$

$$\langle \Delta D_{ABS} \rangle_{global} \pm \sigma(\langle \Delta D_{ABS} \rangle) \leq 5\% \pm 5\% \tag{9}$$

If either criteria is not met, further investigations are needed (Elia, 2019, pp. 69-72).

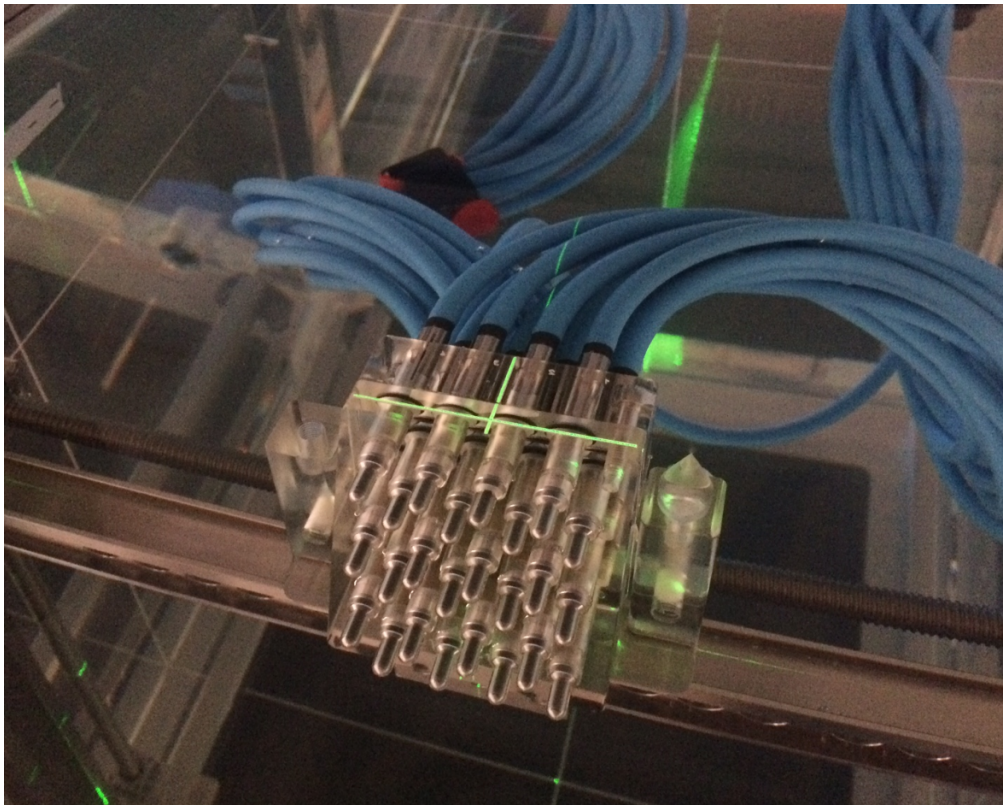

Figure 8: 3D-Block containing 24 PP ionization chambers. Arranged in a configuration that avoids shadowing effects between the PPs (Elia, 2019, p. 71). Image from (Carlino, 2018a, p. 24)

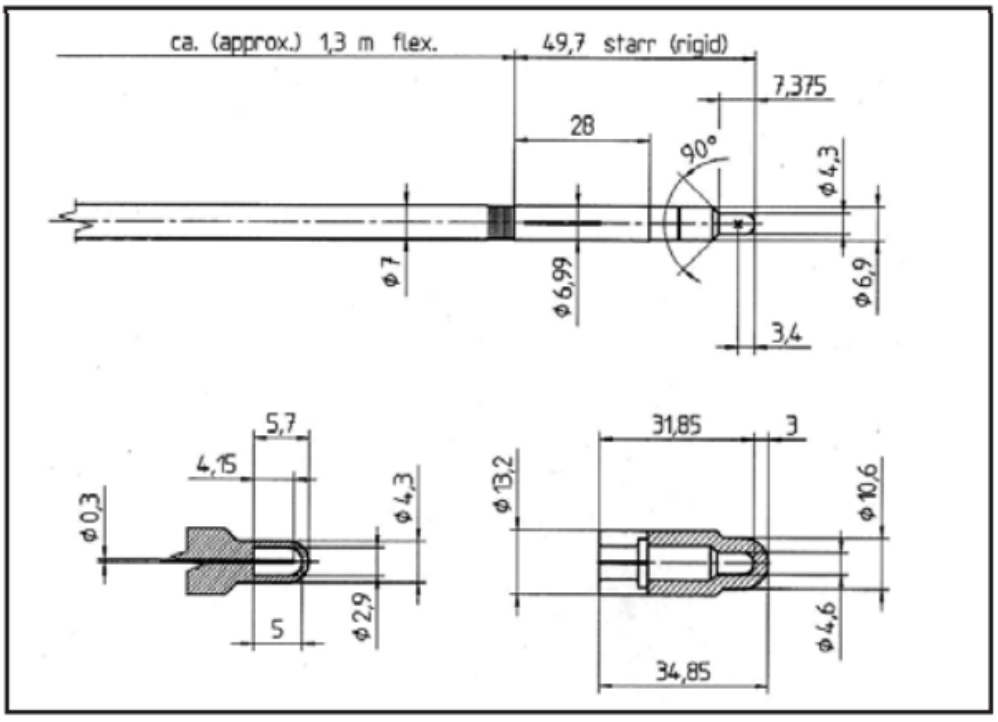

Figure 9: Dimensions of PTW TM31015 ionization chamber. The PPs have a volume of 0.03 cm^3 and allow for quasi-punctual measurements (Elia, 2019, p. 71). Image from (PTW, 2020, p 58)

1.6 The Monte Carlo-method in proton beam therapy dose calculation

According to Paganetti et al. (2008) Monte Carlo-algorithms are generally considered to be the Gold Standard in the dose calculation of ion beam therapy. In contrast to analytical approaches, Monte Carlo simulations utilize theoretical models or experimentally determined cross-sections to account for interactions of individual particles. Furthermore, Monte Carlo-algorithms track secondary particles such as nuclear fragments. Additionally, they take inhomogeneities in the target material into account by modelling the specific properties of materials, such as electron densities and ionization potentials. Many proton treatment facilities have an interest in developing their own Monte Carlo-based dose calculations (Paganetti et al., 2008, p. 4826).

The use of Monte Carlo-based dose engines over conventional algorithms can potentially reduce range uncertainties. This is largely due to a more accurate accounting of range degradation caused by Multiple Coulomb Scatterning (MCS) due to inhomogeneities in the beam path (Paganetti, 2012, pp. 111-112).

Sawakuchi et al. (2008) studied complex inhomogeneities perpendicular to the beam direction. The changes in density change the energy spectrum of the proton fluence and decrease the steepness of the distal fall-off of the Bragg Peak. This can be seen in figure 10. The distal fall-off represents the decline from 80 % to 20 % dose. A failure to take this range degradation into account could lead to a needless exposure of healthy tissue after the tumor or a heterogeneous dose distribution in the target (Sawakuchi et al., 2008, p. 4606).

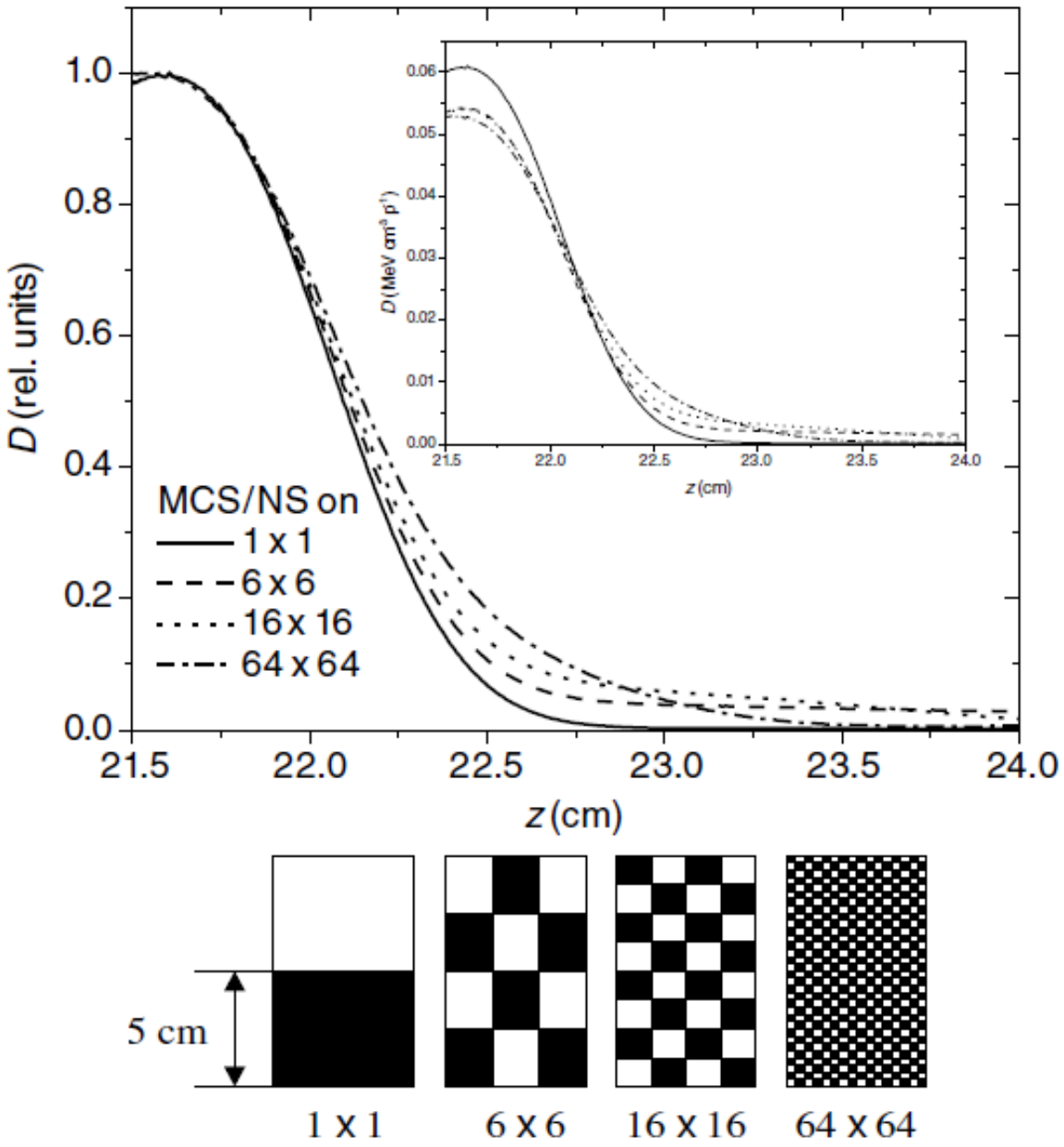

Figure 10: Range degradation at Bragg Peak distal fall-off. Monte Carlo simulation of a 220 MeV proton beam passing through mosaic-like slabs of different complexity (1x1, 6x6,...) including multiple Coulomb scattering and nuclear scattering. Image adapted from Sawakuchi et al. (2008)

Soukup et al. (2005) performed a comparison of MC dose calculation and an analytical pencil beam algorithm. One of the cases analyzed is a heterogeneous material parallel to the beam path. This can be seen in figure 11. A virtual phantom is equipped with a section of bone- and lung-equivalent material and consists of soft-tissue otherwise. The pencil beam passes through the interface. Conventional pencil beam algorithms fail to take this sort of inhomogeneity into account properly. The accuracy of the pencil beam algorithm, however, can be increased significantly by decomposing the beam into sub-spots (Soukup et al., 2005, p. 5100). The resulting

depth dose profile computed with MC shows a double Bragg-Peak, as part of the beam passes through bone-equivalent and part of it through lung-equivalent material.

Analytical dose engines approximate the tissue as thin layers of homogeneous material stacked together, which limits the accuracy of the dose calculation. An advantage of pencil beam algorithms, however, is their superior computational speed (Saini et al., 2017, p. 7660).

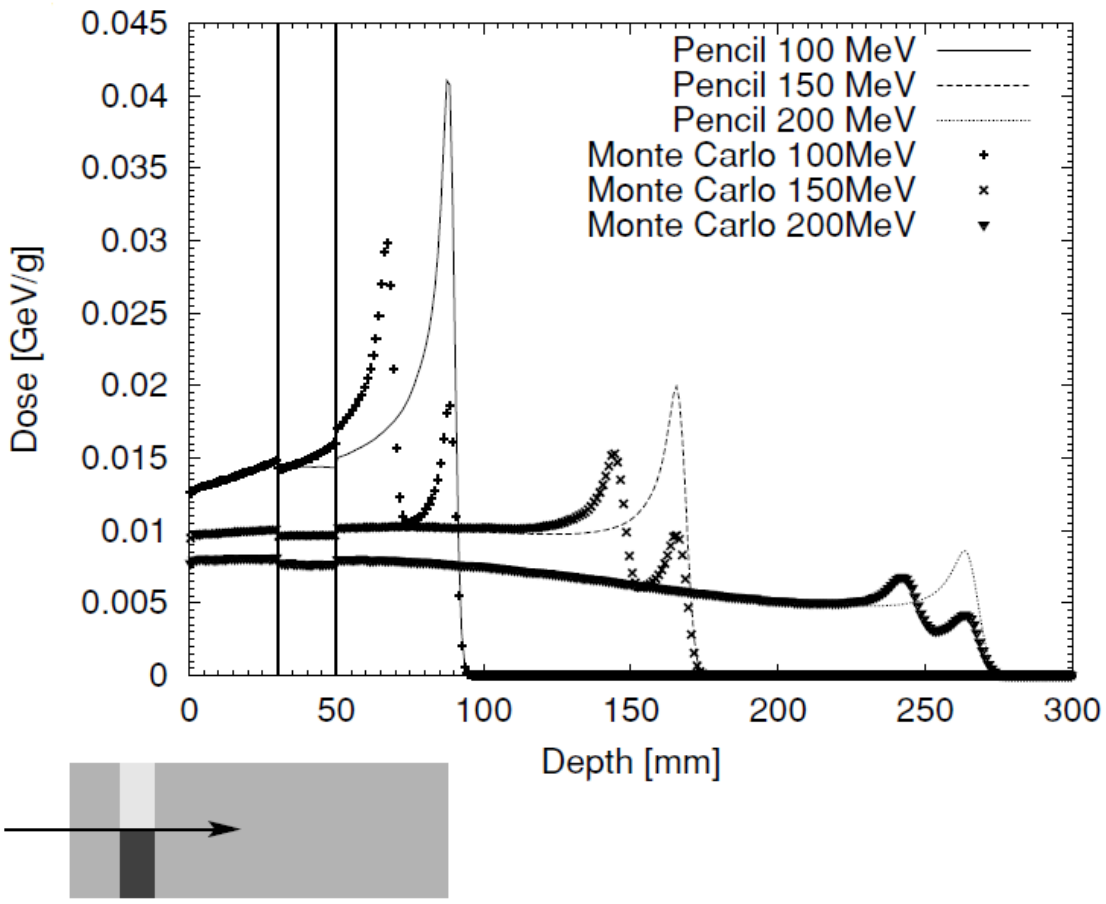

Figure 11: Depth dose distribution in the presence of a bone- and lung-equivalent interface between 3 and 5 cm of depth shown in the lower left and indicated in the plot by the vertical lines. A 100/150/200 MeV beam encounters the interface parallel and centered. Computed with a MC dose engine (VMCpro) and a pencil beam algorithm without sub-spot decomposition. Image adapted from Soukup et al. (2005)

Saini et al. (2017) compared MC dose engines, with an analytical pencil beam algorithm as well as with measurement. The MC tool GATE as well as a commercial MC engine developed by *RaySearch Americas Inc.* are used. The pencil beam algorithm was also developed by RaySearch. One of the cases investigated is the performance of these algorithms in the presence of a range shifter and an oblique incidence of the beam. This can be seen in figure 12.

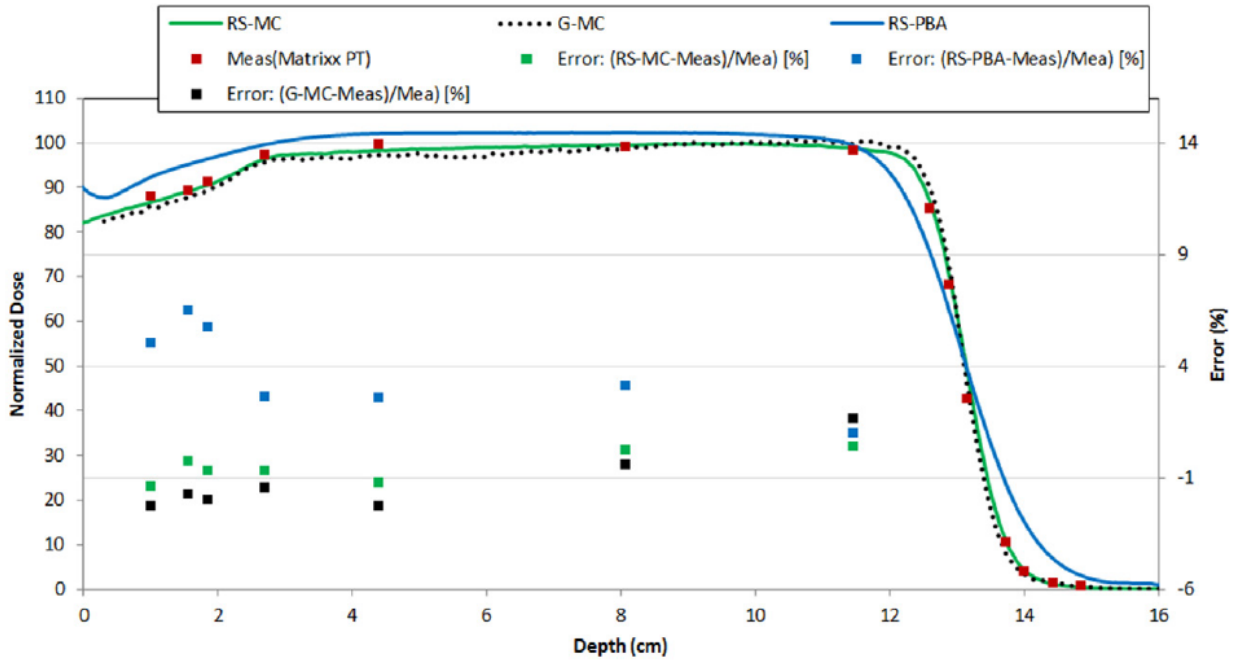

Figure 12: Depth dose profiles computed with MC tools (RS-MC and G-MC) and a pencil beam algorithm (RS-PBA) in comparison with measurement. A range shifter was employed and the beam enters the water phantom at a 45° angle. The squares represent the dose differences relative to the measurements. Image from Saini et al. (2017)

It can be seen that the regions, in which the MC algorithms show better agreement with measurement than the analytical one are in the entrance region of the SOBP, which is likely due to the dose build-up due to secondaries (this can also bee seen in figure 13), and in the distal fall-off of the SOBP. This is likely due to the oblique incidence of the beam.

Another significant uncertainty in dose calculation, specifically in the calculation of stopping power is caused by the approximation of the mean excitation value I, which represents one of the two factors in Bethe-Bloch-equation (1) that is responsible for the linear energy loss of the primary particles. This effects both Monte Carlo and analytical dose engines (Paganetti, 2012, pp. 111-112).

In proton therapy most of the energy deposited in the tissue occurs through ionization and excitation, followed by nuclear interactions. MCS contributes the most to the broadening of the beam. The different types of interactions are implemented based on experimental data, models and parameterizations. The nuclear cross-sections in dependence on proton energy have to be approximated in some cases, as they are not known for all reaction channels. As a rough estimate it can be said that about $1\,\%$ of primary particles undergo nuclear interactions per centimeter (Seco and Verhaegen, 2013, p. 202).

Paganetti (2002) analyzed the influence of nuclear interactions in proton therapy. The reduction in proton fluence due to nuclear interactions influences the depth dose distribution significantly. Furthermore, secondary protons resulting from nuclear interactions contribute to the dose build-up of the Bragg-curve and to the entrance region of the SOBP (See figure 13).

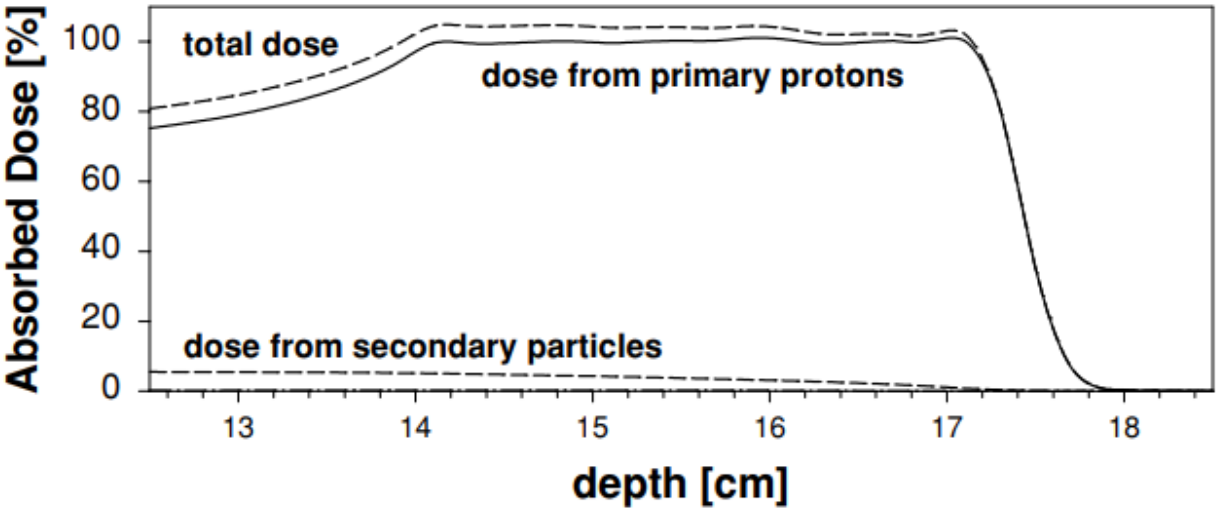

Figure 13: Contribution of secondary protons to SOBP. Monte Carlo simulation of 160 MeV proton beam in water. Image from (Paganetti, 2002, p. 757)

The total dose contribution of nuclear fragments heavier than protons is small. This can be seen in figure 14. Secondary protons and α-particles do, however, factor into the estimation of the radiobiological effectiveness. MC calculations of the dose resulting from secondary neutrons is below 0.04 Gy at a distance of 2 cm downstream of a 3-3-3 mm SOBP (at 160 MeV in water) and the induction of secondary tumors resulting from such an exposure is estimated to be negligible (Paganetti, 2002, p. 762).

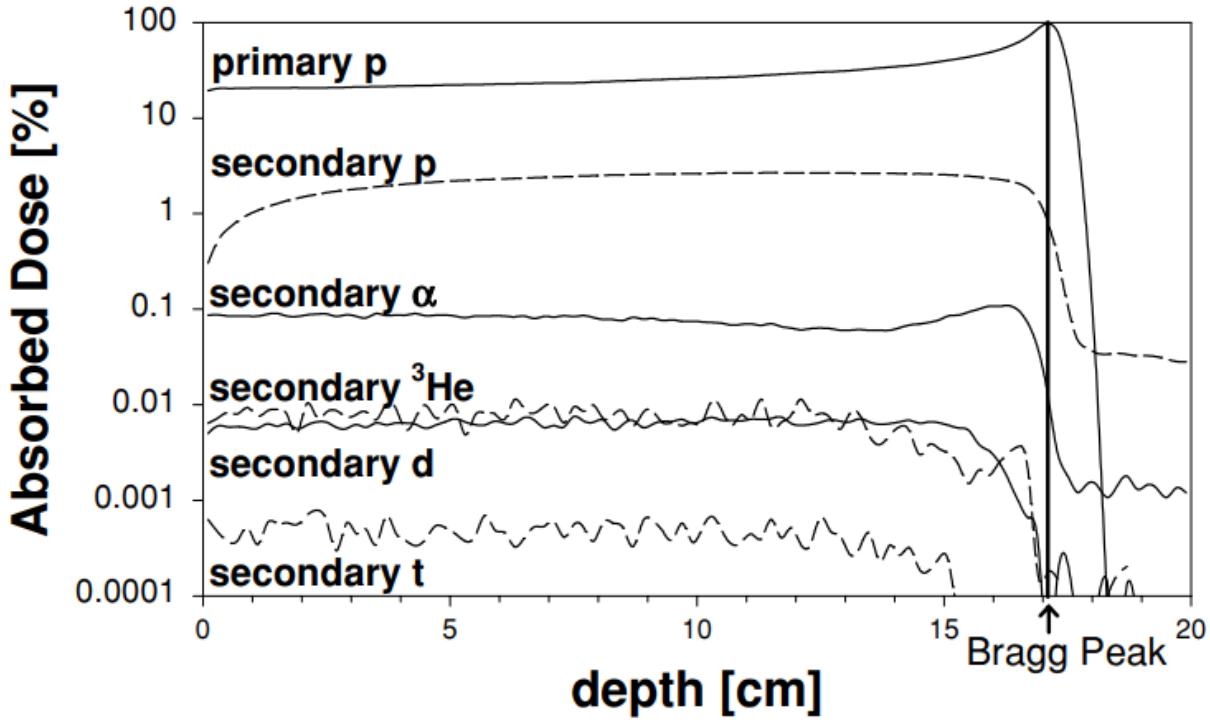

[H]

Figure 14: Monte Carlo simulation of a 160 MeV proton beam in water. Relative absorbed dose (logarithmic scale) due to various nuclear fragments as a function of depth. Image from (Paganetti, 2002, p. 756)

The consideration of nuclear interactions plays a particular role in pencil beam scanning, because each pencil is surrounded by a low-dose envelope ("halo"). For high energy beams this is mostly due to secondary particles resulting from non-elastic nuclear interactions and for low energy beams it is mostly due to nuclear scattering (Sawakuchi et al., 2010, p. 720).
The nuclear interaction cross section peaks at about 20 MeV and declines rapidly afterwards, the contribution of nuclear interactions can therefore be neglected after the pristine Bragg-Peak. The proton energy at the Bragg-Peak is roughly 10 $\%$ of its initial energy (Seco and Verhaegen, 2013, p. 211).

Delta electrons from a 250 MeV proton beam have a maximum range of 2.5 mm, whereby the highest energy electrons are ejected in beam direction. The majority of delta electrons have a range below 1 mm in water, which makes their tracking unnecessary in most cases (Seco and Verhaegen, 2013, p. 202).

When simulating the dose to the patient, a statistical uncertainty of less than 2 $\%$ for the target volume is advised (Seco and Verhaegen, 2013, p. 208). The Monte Carlo method in a clinic

can be used to gain additional information and to double-check the dose predicted by analytical algorithms (Paganetti et al., 2008). It can also be used in the validation of analytical algorithms as well as the commissioning of treatment planning systems (Newhauser et al., 2007).

The most common general purpose codes include *FLUKA*, *Geant4*, *PHITS* and *MCNPX*. In addition, programs such as *GATE* were developed as object oriented toolkits that serve as interfaces of the general purpose codes and do not require extensive programming skills for the user (Elia, 2019, p. 6).

1.7 GATE/GEANT4

The toolkit **GE**ometry **AN**d **T**racking **4** (GEANT4) is a C++ Monte Carlo based algorithm developed at CERN. It was originally designed for high energy physics applications, it therefore contains the information on a large number of particles, models and cross-sections needed to simulate high energy collisions. It is up to the user to select and adjust the various simulation parameters for their own applications (Grevillot, 2011, p. 7).

The **G**eant4 **A**pplication for **E**mission **T**omography or GATE is a platform for Monte Carlo simulations developed by the OpenGATE collaboration[3]. It represents an interface for GEANT4 and was initially used for imaging simulations. The main advantages of GATE lie in its versatility, it allows the management of simulation times and the definition of complex geometries. GATE is updated regularly to stay compatible with GEANT4 releases (Grevillot, 2011, p. 8).

With the release of GATE V6 in 2010 the capabilities of GATE have been extended to allow for simulations of radiotherapy applications (Jan et al., 2011).

GATE-RTion is a long term GATE release for pencil beam scanned ion beam therapy centers (Grevillot, 2019, p. 39).

1.8 IDEAL and ROS

The measurement based PSQA described in section 1.5 currently represents the only way to check whether a treatment plan can be delivered with sufficient accuracy. There are drawbacks to this PSQA process however. The measurement of the dose in a water phantom for example, does not provide any information on the dose distribution within the patient. Furthermore, the PSQA process requires substantial beam time that could be reallocated toward patient treatment (Elia, 2019, p. 68).

At MedAustron it requires roughly 1 hour of machine time per patient to perform the PSQA process. It is therefore planned, to partially replace this experimental PSQA process of irradiation

[3] http://www.opengatecollaboration.org

of a water phantom by an Independent Dose Calculation (IDC) system based on the Monte Carlo method (software-based PSQA) referred to as IDEAL (**I**ndependent **D**os**E** C**A**lculation System for **L**ight Ion Beam Radiotherapy) (Grevillot L. and Stock M., personal communication, June 22, 2020)).

It is developed by MedAustron in collaboration with ACMIT GmbH and the Medical University of Vienna. The project is funded by the Austrian Competence Centers for Excellent Technologies (COMET) program (Grevillot, 2019, p. 40). IDEAL is based on GATE-RTion1.0 and GEANT4 10.03p3 and is not limited to proton dose calculations. It is planned to be used for carbon ion plans as well. The particle histories can be tracked starting at the vacuum window, meaning the entire nozzle including all components is modeled (Grevillot L., personal communication, April 14, 2020). The components of the treatment head can be seen in figure 5.
The output of IDEAL is a three dimensional dose distribution calculated based on the Monte Carlo-method and the beam parameters for a given treatment plan or patient CT information. This dose distribution is saved as a DICOM-DOSE file, which is a data-format commonly used for medical applications. It basically contains all the relevant information on the patient, the scoring resolution, a timestamp, etc. as well as the three dimensional image.

In order to implement any medical software or equipment for clinical use, it has to be commissioned. This means that its functionality and accuracy has to be characterized over the entire spectrum of possible operation (Carlino, 2017, p. 45). In the case of IDEAL, this means it has to be compared extensively with measurement. The commissioning process of IDEAL is threefold. There is 1D, 2D and 3D commissioning.

The 1D commissioning aims to determine the capabilities of IDEAL in reproducing the dosimetric properties of a single static pencil beam. The second part, the 2D commissioning evaluates mono-energy layers with multiple spots (Carlino, 2018b, p. 8). This work discusses the 3D-part of this process, which is similar to the PSQA procedure described in section 1.5. The measurement set-up is identical and the IC measurements are evaluated against IDEAL-generated doses in terms of local and global dose differences. In order to extract the 24 PPs from the IDEAL-computed dose distribution and to evaluate them against the 24 PP measurements in terms of the criteria introduced in 1.5, a Python tool, referred to as ReadOutScript (ROS) has been developed. The ROS has been developed in accordance with the IEC 62304 standard. It allows for reliable feedback for the development process of IDEAL and is planned to be used for its later commissioning. The use of the ROS is not limited to IDEAL and can be used more generally in

combination with any dose calculation system given the proper input parameters. In parallel to this tool, scripts for the 1D and 2D commissioning are being developed at MedAustron. All three are implemented under one graphical user interface to form the Toolkit for Evaluation of DICOM Doses (TEDD). The ROS has been developed for the fixed horizontal-beam-line at MedAustron. It has been implemented and tested by using proton dose distributions. The purpose of this master thesis is to report on the development, validation, first application and results of the ROS.

2 Material and methods

2.1 ReadOutScript

2.1.1 Implementation

The ROS reads a given DICOM-file and extracts the three dimensional dose distribution as well as other relevant specifications. It then reads an xlsx-file generated by PlanVerificator. PlanVerificator is a MedAustron-developed program, which represents the interface between the treatment planning and the measurement equipment in the water phantom. This contains the measurements performed with a phantom and 24 ionization chambers, the position of the detector within the phantom as well as other relevant specifications and analysis. The ROS reads the location of the detector, defines the 24 points of interest accordingly and interpolates the doses at these 24 points. Figure 15 shows the workflow of evaluating IDEAL dose distributions and the role of the ROS in this process.

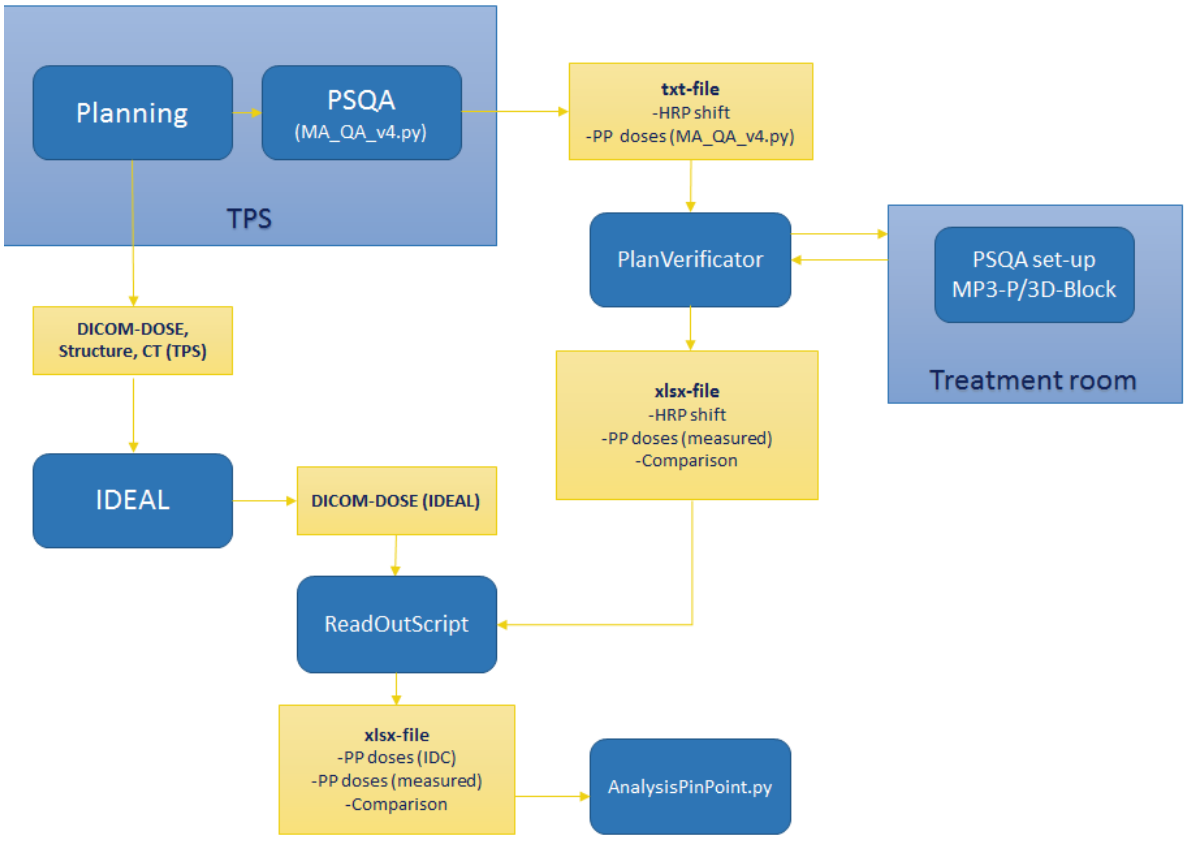

Figure 15: Workflow for the 3D commissioning of IDEAL. The "MA_QA_v4.py" is the already validated script for the extraction of the 24 PP-doses, which is implemented in the TPS

The ROS uses point-like linear interpolation. It calculates the same parameters as introduced in section 1.5 with the notable difference that the measured dose serves as a reference instead of

the computed dose as during the PSQA procedure. The number of ICs N is generally 24 for a given measurement. However, in some cases ICs were inactive or showed unusual behavior during the experiment, in which case the ROS disregards the measurement from the analysis. The ROS was written such that it can be used via command line or via a GUI, which can be seen in figure 16.

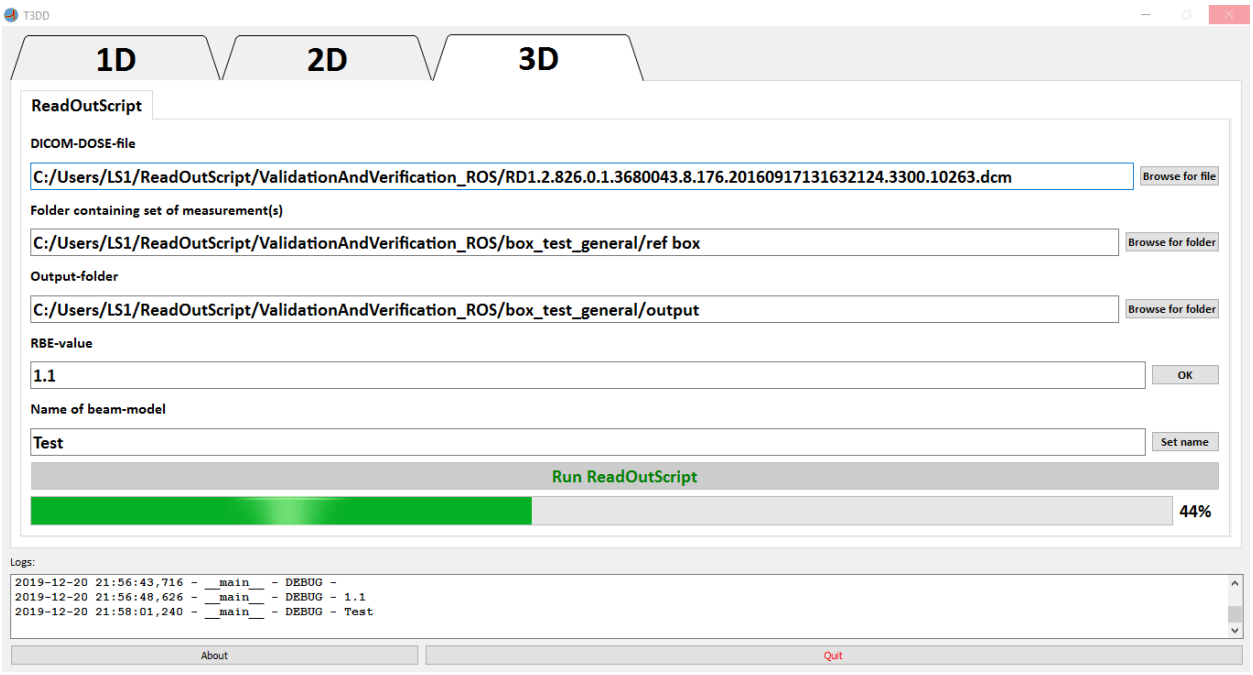

Figure 16: Graphical user interface for the 3D-part of TEDD. The first two lines specify the file path to the dose distribution and the measurements, the third specifies the folder in which the output and log-file should be saved. The RBE-value can be chosen freely, as some input files use physical and others RBE-weighted dose distributions. The "Name of beam-model" is needed for compatibility with existing scripts

The output-files are formatted in a particular way to allow for compatibility with already existing scripts, namely the "AnalysisPinPoint"-script, which is being used for a majority of the plots in this thesis. The output-files are made up of two parts, the first is a header, which contains all the specifications, such as the HRP-shift[4], a timestamp, the plan-name and the second contains the extracted and measured doses as well as the analysis. The first and second part of the output file are shown in figures 17 and 18, respectively. Along with the output-file, the ROS exports a log-file with all relevant parameters. An example of a log-file can be seen in figure 19. It repeats this process sequentially for a set of measurements. To ensure that the correct beam-line, detector and files were used, the ROS employs several safety features. If any criteria is not met, the name of the output-file is flagged and it is noted in the log-file.

[4]The Holder Reference Point shift (HRP-shift) defines the position of the detector during the measurement

1	Plan Verificator version	1.1.0.0
2	User	aut
3	Computer	10.2.57.79
4	Report creation	25.10.2019 16:52
5	ReadOutScrip	1.0
6	Patient ID	QA_PS-01
7	Patient Name	Comm_3D_MP3^Ref-boxes_2016-09
8	Plan name	Box 6 (0,0,6) ISD0cm ref
9	Beam Set Name	Box6 (0,0,6)
10	Prescribed biological dose (Gy[RBE])	1,1
11	Particle Type	Protons
12	Machine Name	IDEALv9.0 (2.7% scaling)
13	Beam Line	Horizontal
14	Beam Name	Box 6 (0,0,6) ISD0cm ref
15	Couch Angle (deg)	0
16	Gantry Angle (deg)	90
17	RaShi	Out
18	SpotTuneID	4
19	Gap (cm)	64,8
20	Dosegrid (cm)	{'R-L': 0.20000000000000001, 'I-S': 0.20000000000000001, 'P-A': 0.200000000
21	Threshold maximum gradient (Gy/mm)	0,04
22	Maximum % of points above the threshold gradient (%)	0
23	Holder type	3DBlock Holder
24	Phantom type	MP3-PL
25	QA plan name	Box6 (0,0,6)
26	QA plan modification time	29.09.2016 13:40:07
27	Reference POI	Zero_HBL
28	Maximum physical dose per beam (Gy)	1,041
29	HRP Shift	A: 0,2mm, B: 0mm, C: 3mm
30		
31	Calibration file	R:\Medical\Medical Physics\PlanVerificationConfiguration\EBG_calibrati
32	Detector set	Detector set EBG (Configuration of detector set from date: 2016-09-03)
33	Active Multidos	Multidos1 (001595), Multidos2 (001586)
34	ComServer	10.2.57.85
35	Measurement settings	Mode: Charge, Range: Low, Unit: Electrical
36	Measurement start	2016-10-07 05:50:14
37	Measurement end	2016-10-07 05:56:16
38	Air pressure (hPa)	984
39	Temperature (°C)	23,3
40	Measurement holder position	A: 0,2mm, B: 0mm, C: 3mm

Figure 17: First part of ROS-output containing relevant specifications. Cells marked in red are of particular interest either for the safety features, compatibility or dose extraction

41	Gradient (Gy/mm)	D_{comp} (Gy)	D_{meas} (Gy)	ΔD (Gy)	ΔD_{local} (Gy)	ΔD_{global} (Gy)	Inactive
42	0,009	0,85	0,82	-0,03	-3,12	-2,34	FALSCH
43	0,01	0,85	0,82	-0,03	-3,43	-2,59	FALSCH
44	0,008	0,85	0,82	-0,03	-3,47	-2,62	FALSCH
45	0,009	0,86	0,83	-0,02	-2,56	-1,94	FALSCH
46	0,022	0,96	0,92	-0,04	-3,74	-3,17	FALSCH
47	0,022	0,97	0,92	-0,04	-4,42	-3,79	FALSCH
48	0,022	0,97	0,93	-0,04	-4,39	-3,78	FALSCH
49	0,022	0,96	0,93	-0,04	-3,92	-3,35	FALSCH
50	0,003	1,03	0,98	-0,04	-4,27	-3,88	FALSCH
51	0,002	1,02	0,98	-0,04	-4,02	-3,62	FALSCH
52	0,006	1,02	0,98	-0,04	-3,49	-3,15	FALSCH
53	0,006	1,03	0,99	-0,04	-4,01	-3,66	FALSCH
54	0,004	1,02	0,97	-0,05	-5,08	-4,60	FALSCH
55	0,003	1,02	0,97	-0,05	-4,70	-4,26	FALSCH
56	0,004	1,02	0,97	-0,05	-4,45	-4,01	FALSCH
57	0,002	1,02	0,97	-0,04	-4,31	-3,89	FALSCH
58	0,001	1,03	0,97	-0,05	-5,28	-4,81	FALSCH
59	0,001	1,03	0,98	-0,06	-5,68	-5,20	FALSCH
60	0,003	1,03	0,98	-0,05	-5,10	-4,65	FALSCH
61	0,002	1,03	0,98	-0,04	-4,27	-3,89	FALSCH
62	0,001	1,03	0,97	-0,06	-5,89	-5,38	FALSCH
63	0,001	1,04	0,98	-0,06	-5,69	-5,22	FALSCH
64	0,001	1,03	0,98	-0,05	-5,07	-4,64	FALSCH
65	0,002	1,02	0,97	-0,05	-4,72	-4,27	FALSCH

Figure 18: Analysis of individual PPs of a set of extracted and measured doses performed with the ROS. The column "Inactive" indicates if the gradient threshold for a given PP is exceeded that then should be disregarded from analysis. Additionally, the ROS calculates averages and standard deviations. Table shortened for better visualization

```
Reading image:R:\Medical\Medical Physics\QADatabase\PSQA with GATE\PLATONIC\Lu
Reading Measurements: R:\Medical\Medical Physics\QADatabase\PSQA with GATE\PLA
Writing results to: R:\Medical\Medical Physics\QADatabase\PSQA with GATE\PLATC
RBE: 1.127
Name of beam-model: IDEALv9.0 (2.7% scaling)
########################################
Measurement-file: PlanVerifictor_Box 12.6 (0,0,31) ISD0cm ref,C3,B0,A200.xlsx
----------------------------
PatientName_DCM: Comm_3D_MP3^Ref-boxes_2016-09
PatientID_DCM: QA_PS-01
QAPlanName_DCM: Box 12.6 (0,0,_1
----------------------------
PatientName_Excel: Comm_3D_MP3^Ref-boxes_2016-09
PatientID_Excel: QA_PS-01
QAPlanName_Excel: Box 12.6 (0,0,_1
----------------------------
Holder_type: 3DBlock Holder
----------------------------
Reference_POI: Zero_HBL
----------------------------
Saftey check passed!
Voxelsize: 2.0
Hrp-shift: A: 200.0 mm B: 0.0 mm C: 3.0 mm
DoseGridScalingFactor: 1.8420992139876094e-05
Maximum Dose (physical): 1.0711798756759359
Analysis notes:nan
1 out of 1 finished
################################################
Extraction successful
```

Figure 19: Logging for one set of measurement produced by the ROS

2.1.2 Development

Considering that the ROS will be used for clinical commissioning it has to fulfill certain standards regarding its validation and documentation, specified in the IEC 62304 standard. The development process starts with specifying the user requirements. The following are the user requirements of the ROS:

R1.) The ROS needs to be able to extract the 24 pin-point doses from a DICOM-DOSE, as specified in a PlanVerificator-file.

R2.) The ROS shall read a PlanVerificator-file and perform a comparison of the extracted and measured doses.

R3.) The ROS shall provide a user-friendly interface to the user.

R4.) The ROS shall be workflow oriented and be compatible with existing scripts used to automatize the 3D-block analyses.

R5.) The user shall be provided with notification if the selected DICOM-DOSE and PlanVerificator-file were chosen incorrectly.

R6.) The ROS shall produce a log file for every set of measurements recording relevant information.

These are then expanded upon by the technical specification that are needed to fulfill these requirements. Additionally, there needs to be detailed documentation of the implementation.

2.1.3 Validation

In partial fulfillment of the IEC 62304 standard, there needs to be an extensive battery of tests to validate each and every functionality of the script as well as its accuracy. More specifically, there is a validation test for each specification, which amounts to 24 tests. These include verification of correct PP placement, determination of the maximum dose, calculation of analytical parameters, logging, safety features, compatibility, etc. The use of the ROS includes, but is not limited to the validation of IDEAL. Once validated it can be used to validate any dose calculation system in three dimensions using a 3D-Block and a horizontal fixed beam line. All tests are summarized in a document and have to be executed and checked by the responsible medical physicist before it is signed. The validation tests are devised in a way such that the script itself remains unchanged. During and after the validation process the script is "frozen" (read-only-mode). Any further change to the ROS requires a full run of the validation tests. These tests verify that the dose is extracted sufficiently precisely and that all functionalities work properly.

2.1.4 ROS additional validation plans

Apart from the verification tests to ensure proper functionality of the ROS, a more extensive validation run has been conducted with TPS-generated 3D cubes in order to evaluate proper interpolation of doses by the ROS. The PlanVerificator-files contain both the TPS-doses (planned doses) as well as the measurements. For the validation of the ROS we are only interested in the interpolation performance compared to the TPS, which is why the measurements are ignored. The ROS then interpolates the doses from a TPS-generated dose distribution and compares them

to the TPS-interpolated doses. The workflow of the validation for the ROS can be seen in figure 20. This has been done for a variety of homogeneous cubic dose distributions and detector positions.

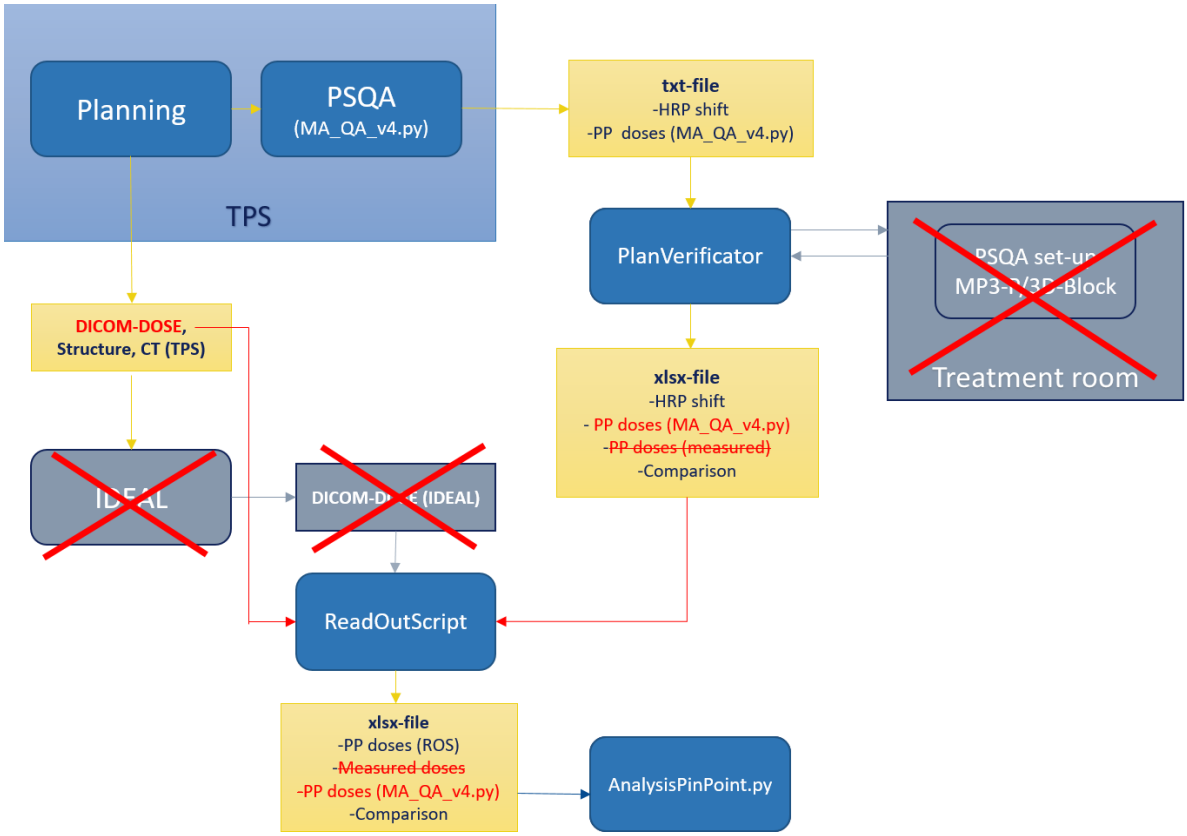

Figure 20: Workflow for the validation of the ROS. The measured PPs are replaced by the MA_QA_v4.py-extracted doses.

Four different cubes of field sizes between 6 (Box6) and 12.6 (Box12.6) cm at Isocenter (ISD0cm) and four 3D cubes of field sizes between 6 (Box6) and 10 (Box10) cm at an Isocenter to phantom Surface Distance of 50 cm (ISD50cm) were used. The isocenter represents a well-defined reference point in the treatment room. A laser system in the room indicates it's position. In clinical practice the target is moved closer to the nozzle. For this reason ISD50cm is used in the validation process. An example of a homogeneous dose distribution can be seen in figure 21.

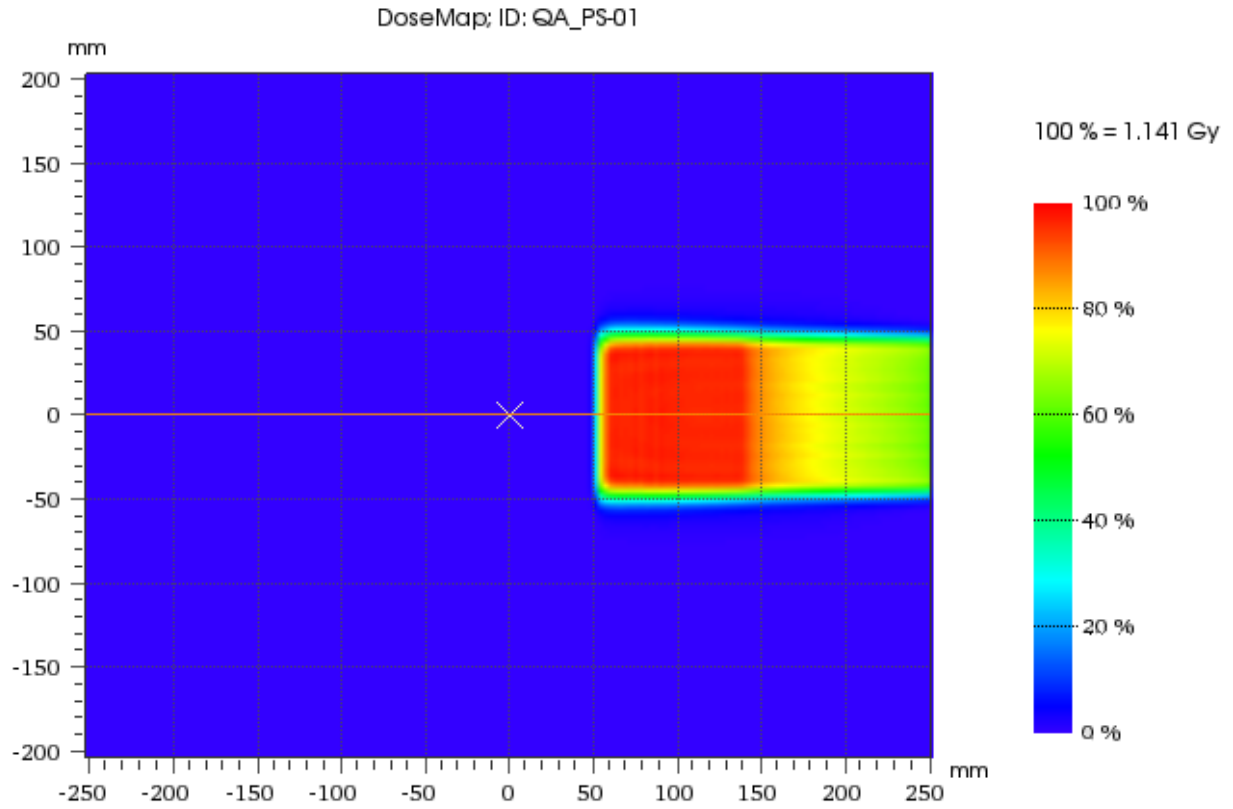

Figure 21: Isodose areas of a TPS-generated homogeneous cubic dose distribution at isocenter with dimensions 8-8-8 cm at a depth of 15 cm. Coronal view. Visualized with PTW-VeriSoft 6.1

In order to validate the ROS for different voxel sizes, an additional four homogeneous spherical dose distributions with scoring resolutions of 1-1-1 mm, 2-2-2 mm, 3-3-3 mm and 1-2-3 mm were produced with the TPS. The ROS-extracted doses were evaluated against the MA_QA_v4.py-extracted doses in terms of global dose difference (24 PPs per plan).

2.2 IDEAL

2.2.1 Evaluation IDEAL0.9 using ROS

The IDEAL-generated dose distributions are evaluated against measurements. These measurements have already been acquired for the TPS-commissioning. The experimental setup and methods by which they were acquired are exactly the same as in the PSQA process described in section 1.5. The workflow of the evaluation is the same as it will be in the commissioning for IDEAL shown in figure 15. A total of 47 proton dose distributions were simulated using IDEALv0.9 and a statistical uncertainty of 1 %, 34 cubic dose distributions at various depths and sizes (including the ones from the validation of the ROS) and 13 irregularly shaped targets both at ISD0cm and ISD50cm. Some of the plans contain a range shifter. The scoring resolution is

2-2-2 cm for all distributions. Irregular targets represent dose distributions with a higher degree of complexity such as H-shaped, L-shaped, cylindrical, etc. plans. Figure 22 shows a visual representation of an L-shaped plan. A full list of the plans can be seen in figure 23. The tracking of neutrons was disabled for these simulations.

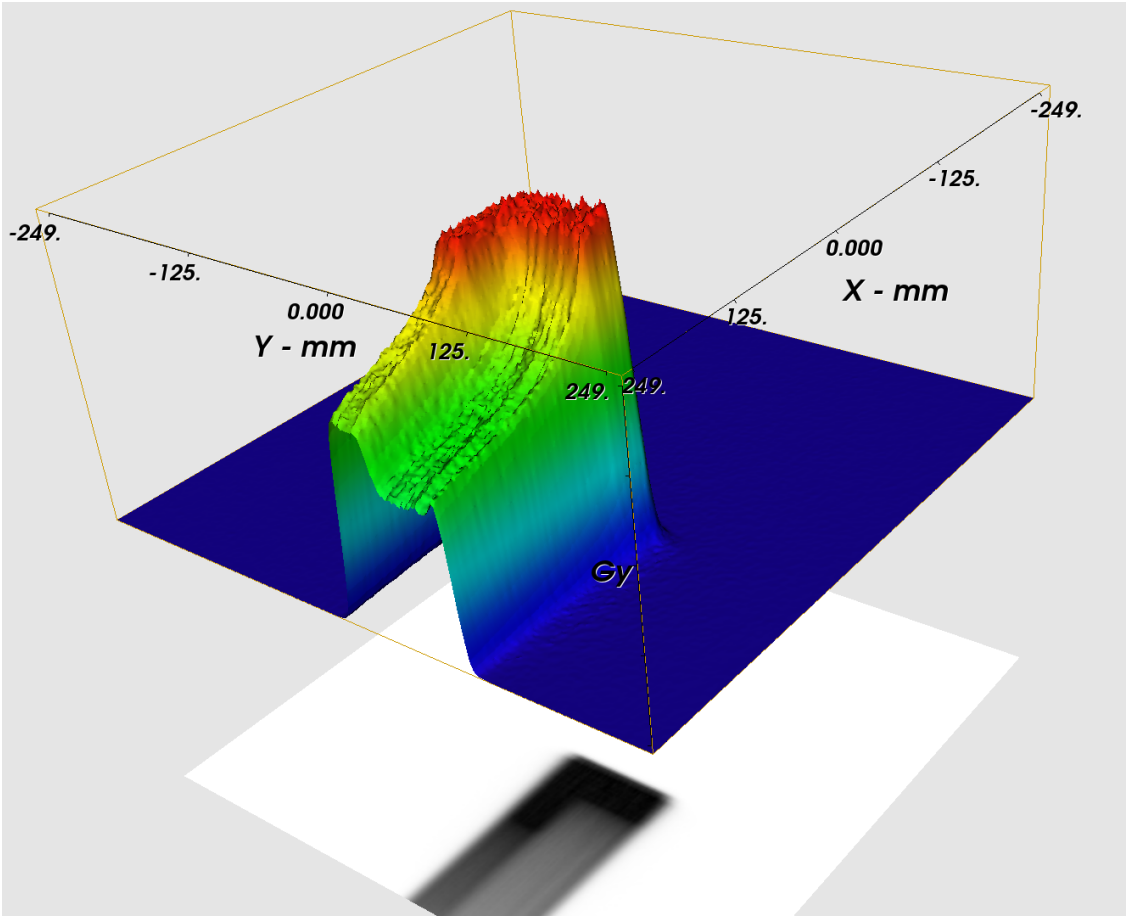

Figure 22: 3D presentation of an IDEALv0.9-generated, L-shaped, off-axis plan at ISD0cm at a slice depth of 81 mm. The X- and Y-axis represent the depth and width in mm, respectively and the third axis the dose in Gy. Visualized with VeriSoft6.1

The results are evaluated in terms mean signed/unsigned global dose differences (5, 6) as is common practice in PSQA and commissioning procedure. Using local dose differences (3) would lead to an over-representation of dose differences in low-dose regions. Unlike in the PSQA procedure, the dose deviations are relative to the measurements, not the computed dose. Another useful metric of evaluating the results are pass-rates, which represent the number of PPs that are within $3\%/5\%/7\%$ global dose deviation as well as directly looking at horizontal- and depth-dose-profiles, which can provide more insight on the shape of the dose distribution. The PPs at a gradient larger than 0.04 Gy/mm and/or a dose below 0.1 Gy were excluded from the analysis as is common practice for commissioning.

	ISD0cm	ISD50cm
3D cubes	Box 6 (0,0,6)	Box 6 (0,0,5) Rashi
	Box 8 (0,0,15)	Box 6 (0,0,6)
	Box 10 (0,0,25)	Box 8 (0,0,15)
	Box 12.6 (0,0,31)	Box 10 (0,0,25)
	Box 3 (0,0,6)	Box 3 (0,0,3.5) Rashi
	Box 20 (0,0,25)	Box 4 (0,0,15) Rashi
	Box 3 (0,0,25)	Box 10 (0,0,25) Rashi
	Box 6 (0,0,15)	Box 20 (0,0,25)
	Box 10 (0,0,15)	Box 3 (0,0,6)
		Box 3 (0,0,25)
		Box 8 (0,0,15) Rashi
		Box 8 (0,0,25)
Irregular targets	3D-L-shape off-axis	Cylinder IS direction Rashi
	Tube IS direction	H-shape cor 90 Rashi
	Cylinder PA direction	L-shape on-axis
	H-shape Coronal	Sphere 6 (0,0,5) Rashi
		Cylinder PA direction
		L- shape on-axis Rashi
		H-shape Coronal 90
		Cylinder IS direction
		L-shape off-axis
		Sphere (0,0,25)

Figure 23: List of IDEAL-generated plans. "Box4 (0,0,15) Rashi" for instance represents a homogeneous cubic dose distribution of dimension 4-4-4 cm with its center at a depth of 15 cm with a range shifter (Rashi) in place. IS stands for Inferior-Superior. In the case of a cylinder this refers to its radial symmetry axis. PA stands for Posterior-Anterior

3 Results

3.1 Validation results of the ROS

A total of 1692 PPs were analyzed for validating the accuracy of the ROS. The PP doses extracted with the ROS are evaluated against the PP doses extracted with the TPS-integrated software (MA_QA_v4). Box6 at ISD50cm includes a Range Shifter (RaShi). Figures 24 and 25 show the depth-dose-curves for a homogeneous cubic dose distribution with dimensions 8-8-8 cm centered at a depth of 15 cm for ISD50cm and ISD0cm, respectively and Figures 26 and 27 show the mean global dose deviations for ISD50cm and ISD0cm, respectively. Figures 28 and 29 show the pass-rates for ISD50cm and ISD0cm, respectively.

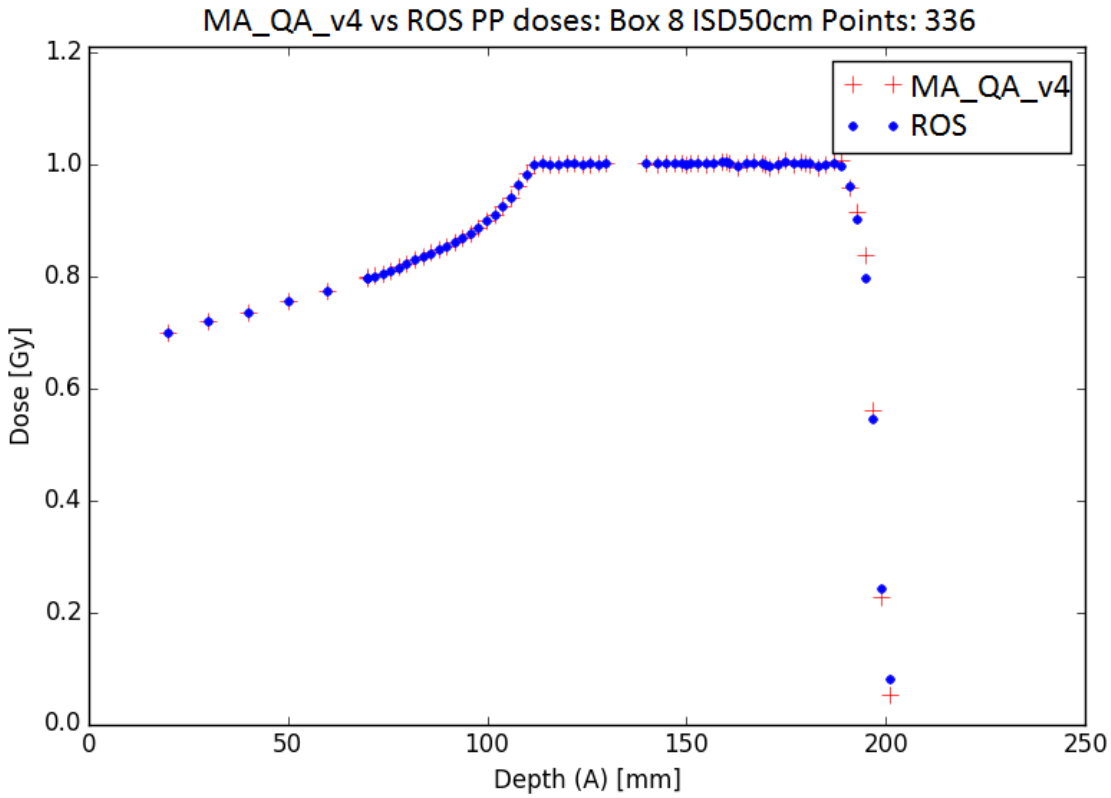

Figure 24: Depth-dose-curve for a homogeneous cubic dose distribution of dimension 8-8-8 mm at a depth of 15 cm at ISD50cm

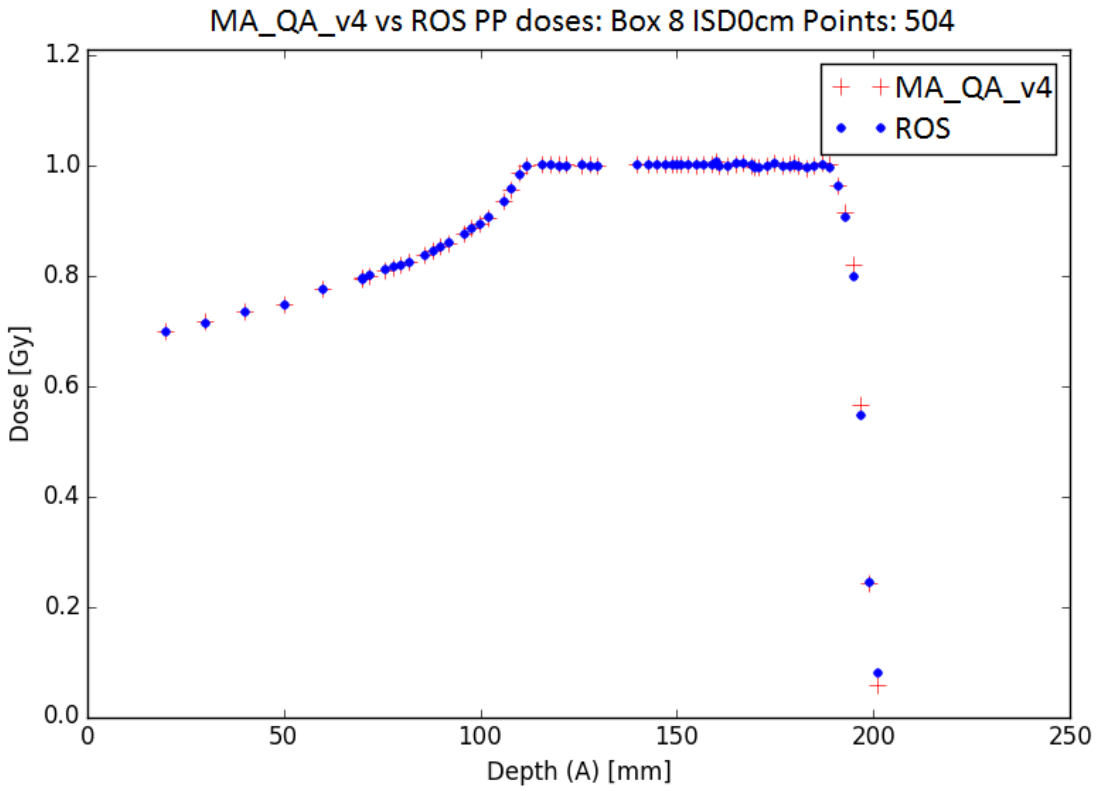

Figure 25: Depth-dose-curve for a homogeneous cubic dose distribution of dimension 8-8-8 mm at a depth of 15 cm at ISD0cm

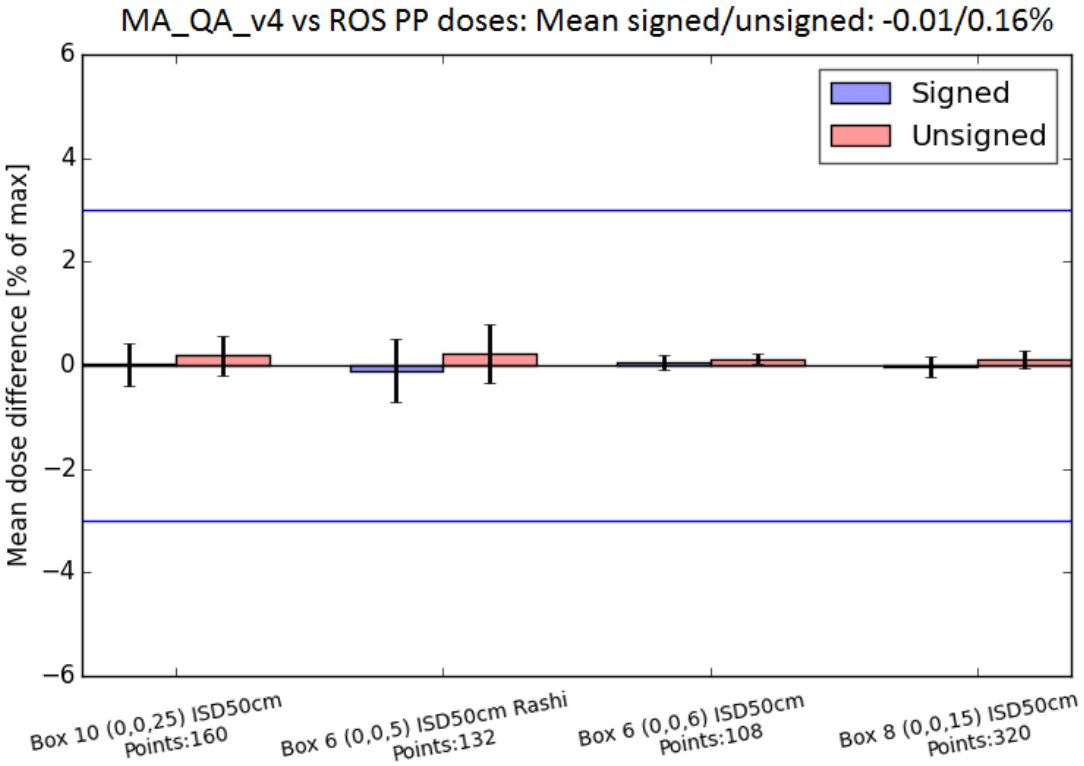

Figure 26: $\langle \Delta D \rangle$ and $\langle \Delta D_{ABS} \rangle$ for plans at ISD50cm. The vertical bars represent the standard deviation of the mean global dose differences. The blue lines represent the 3 % clinical limit

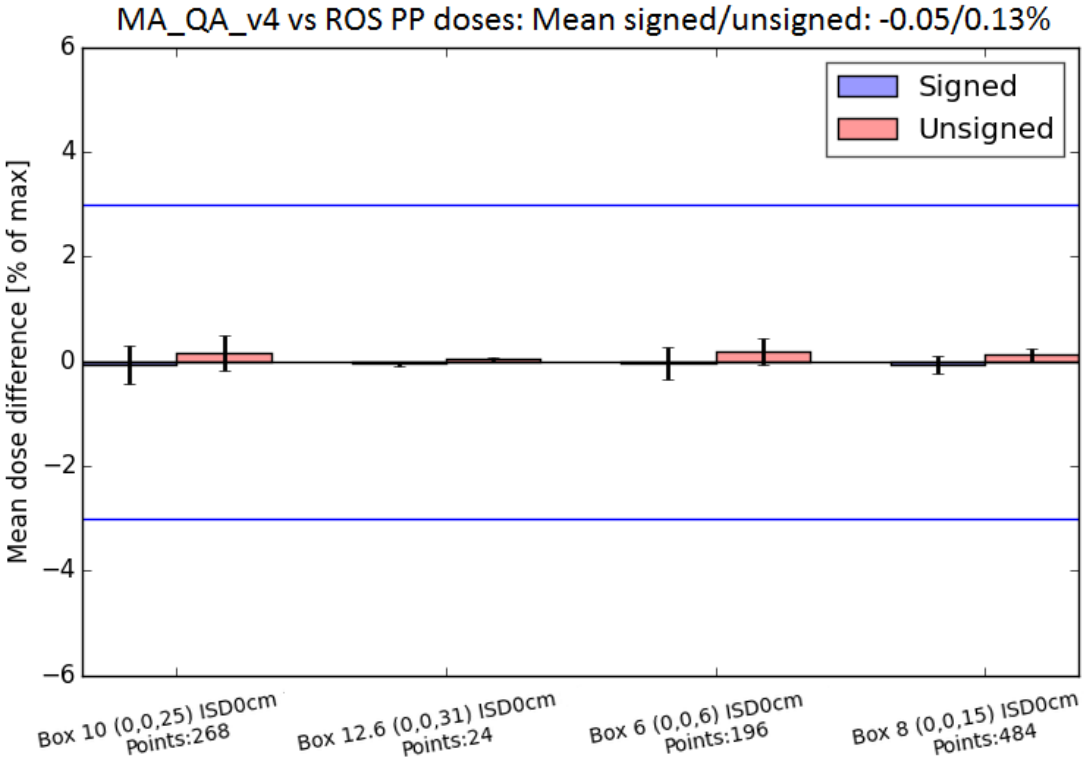

Figure 27: $\langle \Delta D \rangle$ and $\langle \Delta D_{ABS} \rangle$ for plans at ISD0cm. The vertical bars represent the standard deviation of the mean global dose differences. The blue lines represent the $3\,\%$ clinical limit

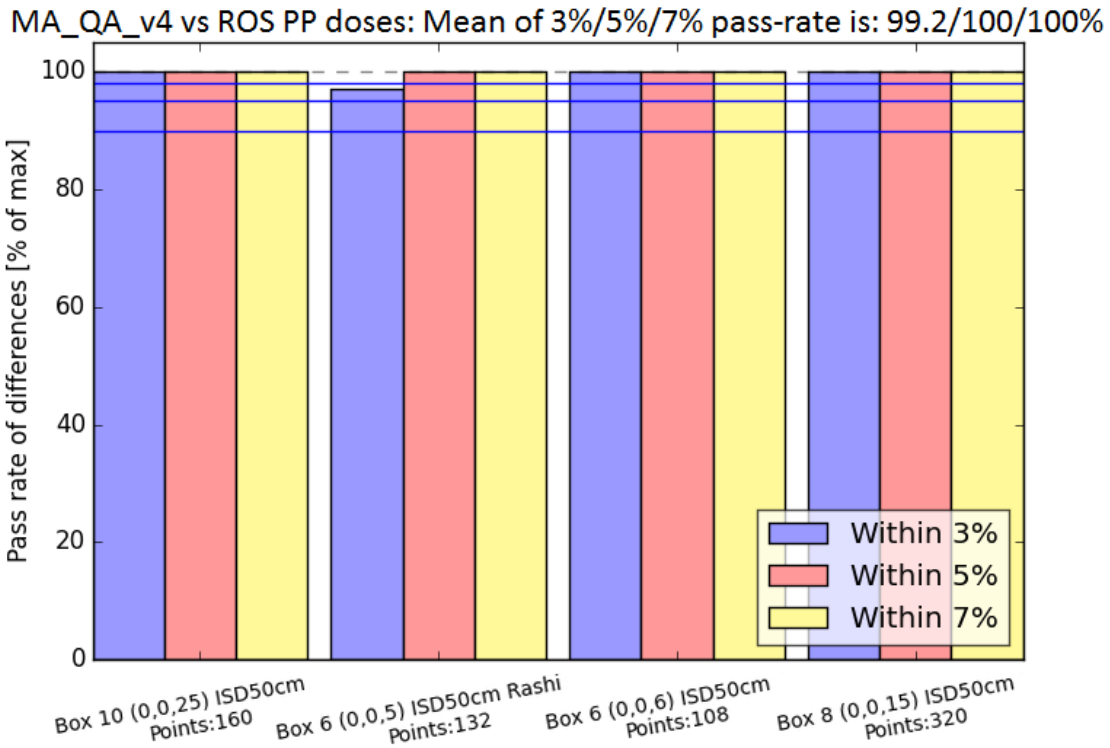

Figure 28: Percentage PPs that agree within $3\%/5\%/7\%$ global dose difference for plans at ISD50cm. The horizontal blue lines represent $98\%/95\%/90\%$. One Box6 includes a Range Shifter (RaShi)

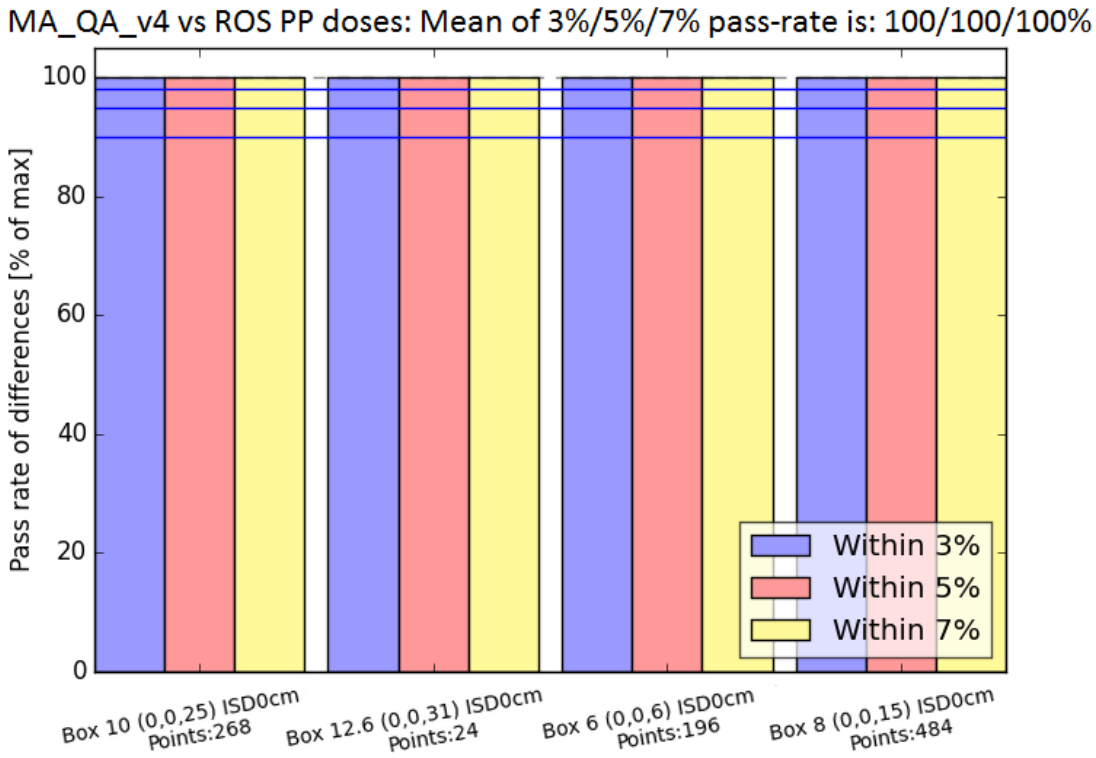

Figure 29: : Percentage of PPs that agree within $3\%/5\%/7\%$ global dose difference for plans at ISD0cm. The horizontal blue lines represent $98\%/95\%/90\%$

Validation scoring resolution: One of the results of the validation for different scoring resolutions can be seen in figure 30, which shows signed global dose differences of 24 PPs for a spherical dose distribution at 1-2-3 mm. The results for 1-1-1 mm, 2-2-2 mm and 3-3-3 mm are almost identical.

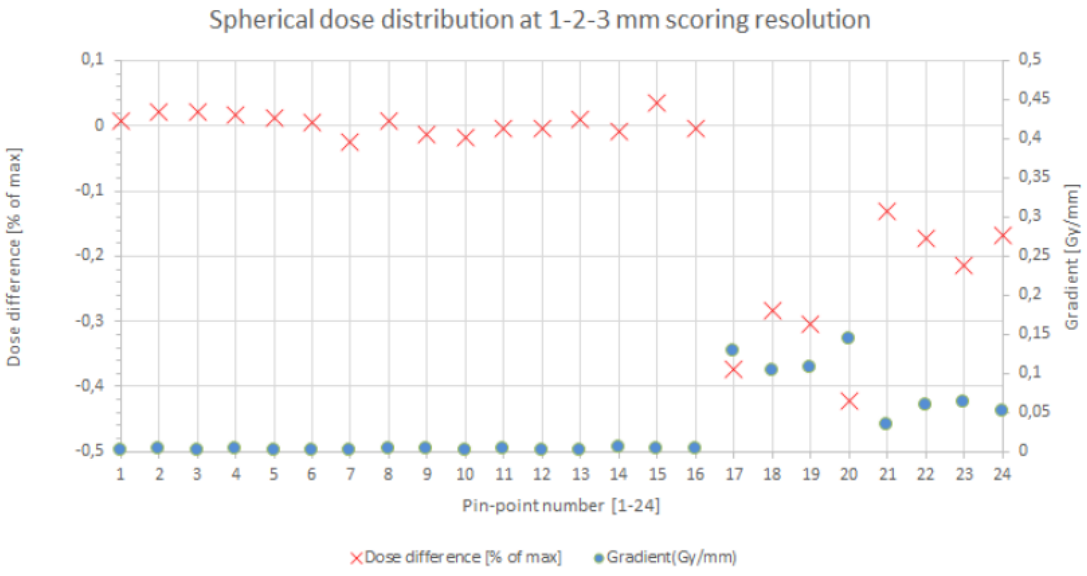

Figure 30: Validation of the ROS for different scoring resolutions. A higher deviation can be seen in the gradient region. The relative dose difference stays within 0.5 %

3.2 Results of IDEALv0.9

A total of 4079 PPs were extracted with the ROS and evaluated against measurement. The first three figures 31, 32 and 33 show the results for the same homogeneous 3D cubic dose distributions (at IDC50cm) as used for the validation of the ROS, in order to illustrate the difference. The latter four figures show an example of the results of irregular targets, namely an L-shaped, an H-shaped, a cylindrical and a spherical dose distribution.

3.2.1 Cubic dose distributions

It can be seen that the pass-rates for Box10, Box6 and Box8 contain global dose differences below 3 % agreement, however, they still show good agreement (Figure 31). The mean unsigned dose deviation remains below 1 % (Figure 32). The depth-dose curve in figure 33 shows a lower measured than simulated dose at the distal edge of the SOBP, this is likely due to the positional uncertainty in the measurement.

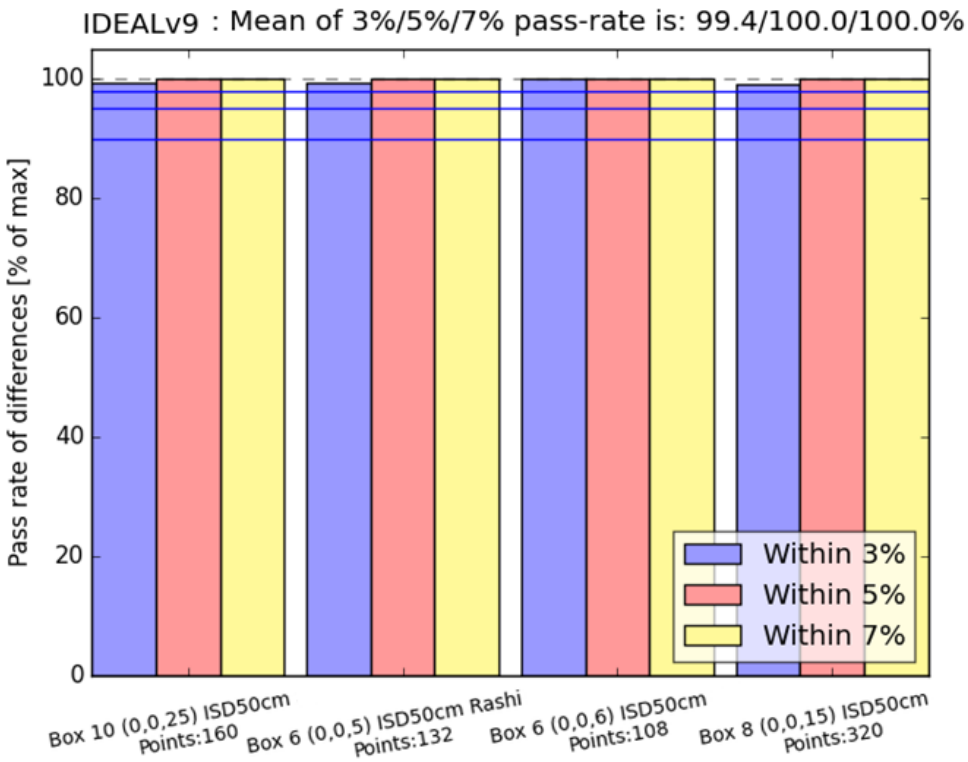

Figure 31: Percentage of PPs that agree within $3\%/5\%/7\%$ global dose difference (measured vs simulated) for cubic dose distributions. The horizontal blue lines represent $98\%/95\%/90\%$. One Box6 includes a Range Shifter (RaShi)

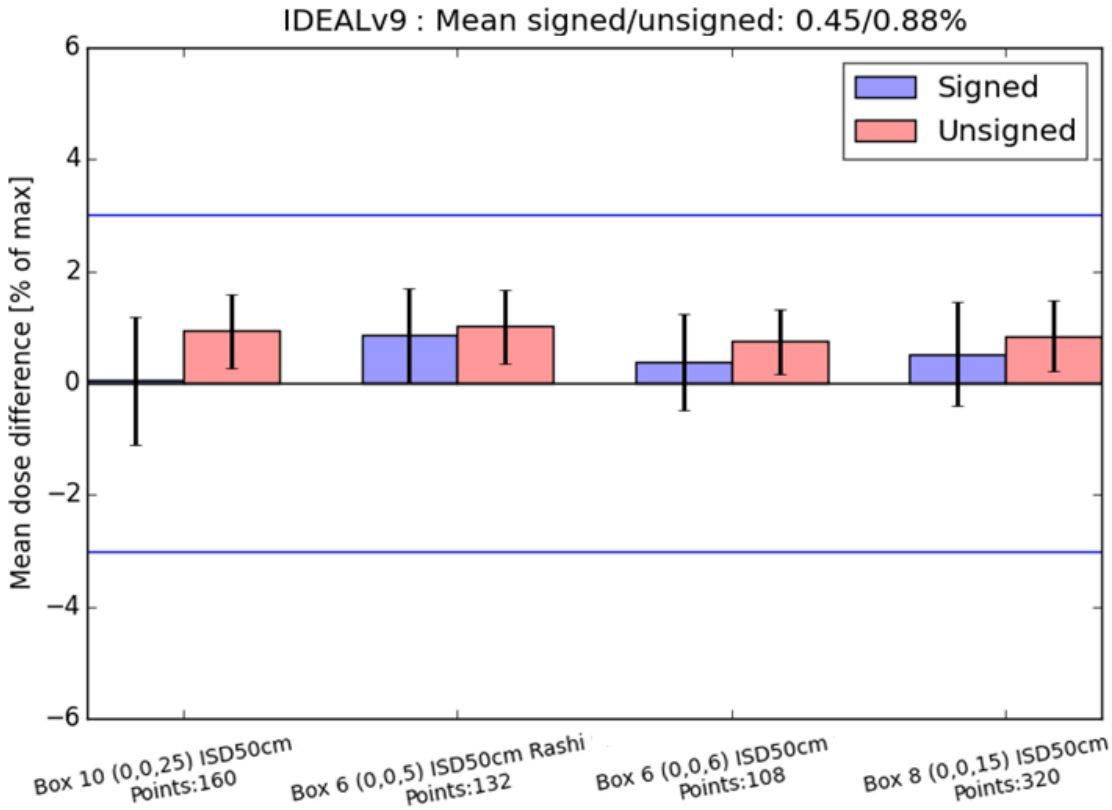

Figure 32: $\langle \Delta D \rangle$ and $\langle \Delta D_{ABS} \rangle$ (measured vs simulated) for 3D cubic dose distributions. The vertical bars represent the standard deviation of the mean global dose differences

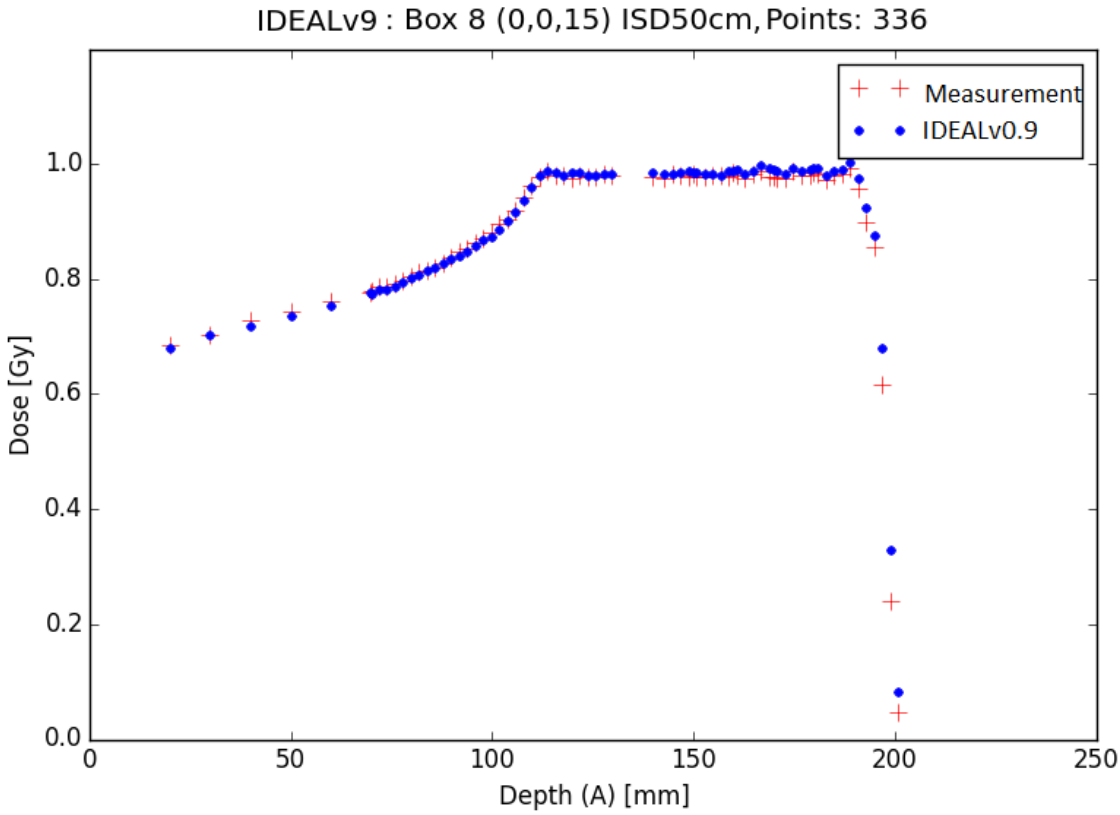

Figure 33: Depth-dose-curve for a homogeneous cubic dose distribution of dimension 8-8-8 mm at a depth of 15 cm at ISD50cm

3.2.2 Irregular targets

Irregularly shaped dose distributions generally contain more gradients. A small offset therefore results in a higher deviation, which is reflected in pass-rates and mean global dose deviations (figures 37 and 36).

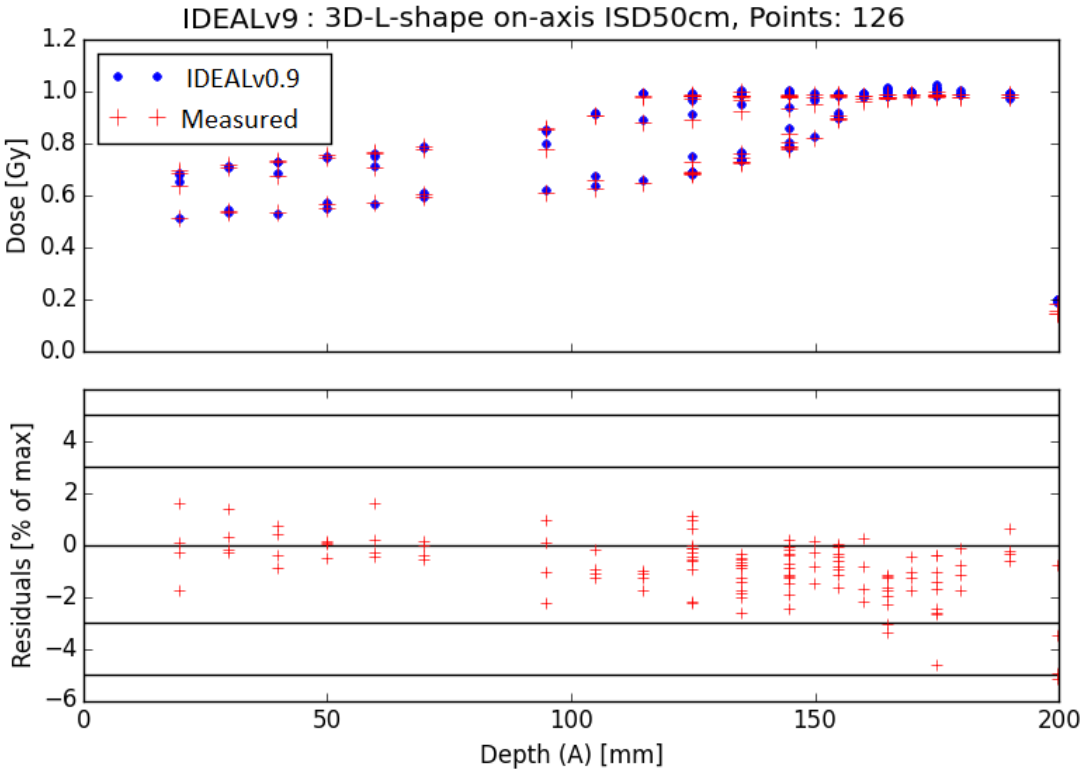

Figure 34: Dose profile of an L-shaped plan at IDC50cm as a function of depth (top), global dose differences for individual PPs (bottom). y range (mm): [-38.2, 38.2], x range (mm): [-7.2, 7.2]

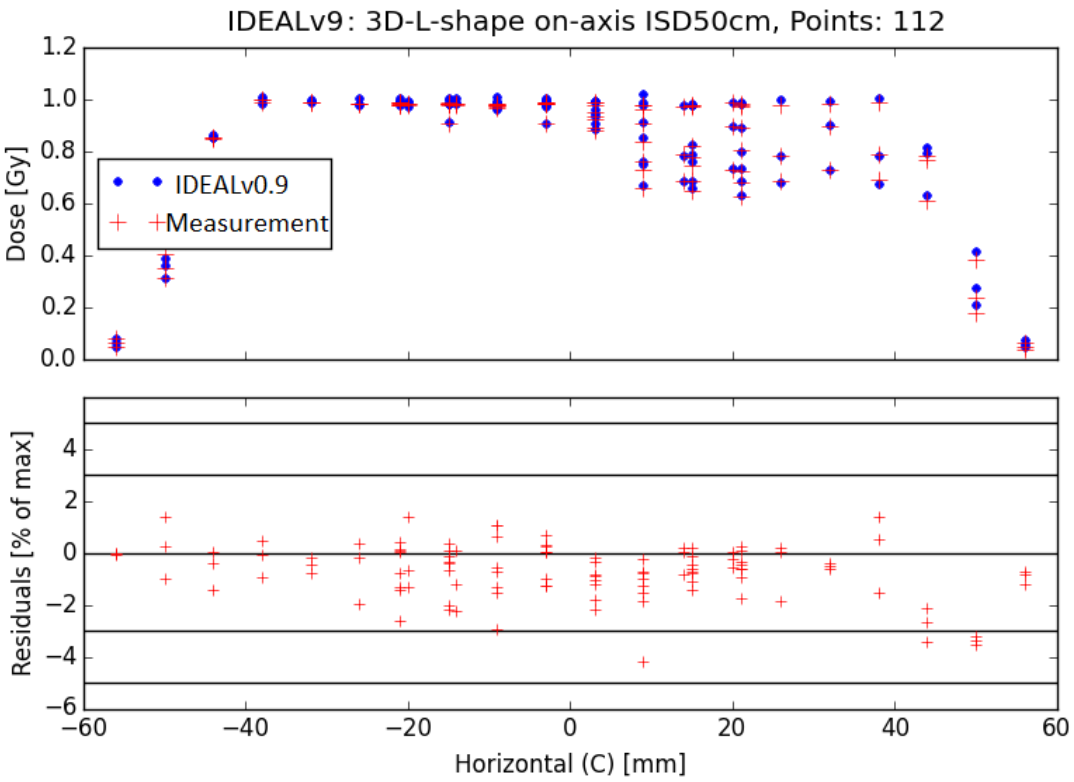

Figure 35: Horizontal dose profile of an L-shaped plan at ISD50cm as a function of distance (top), global dose difference for individual PPs (bottom)

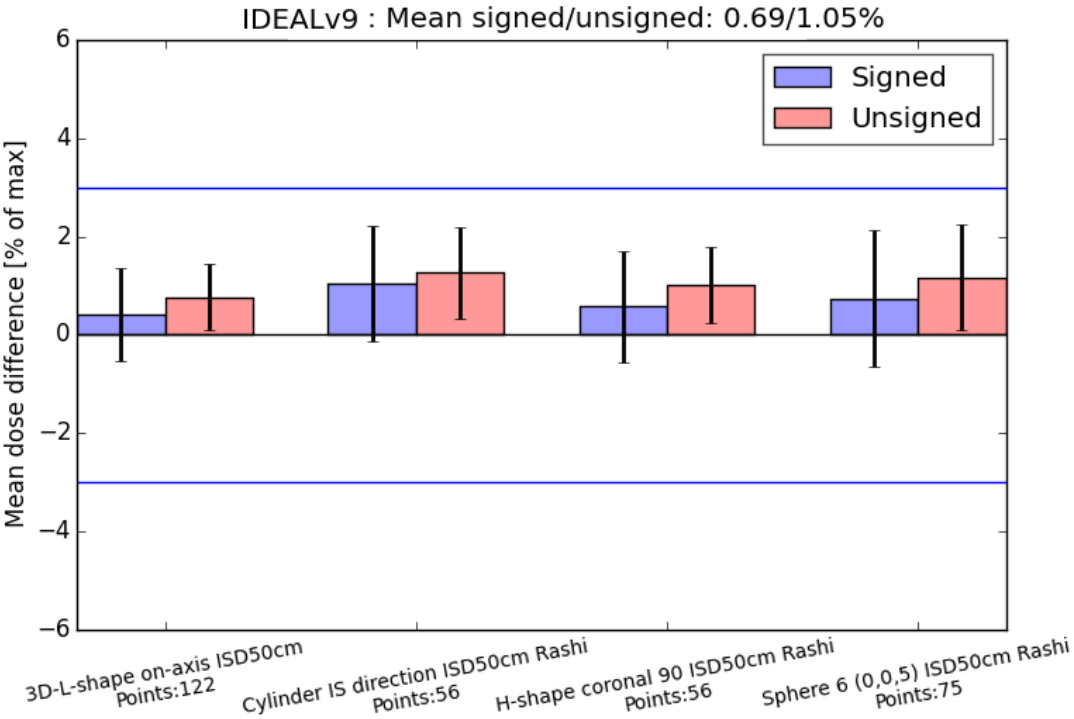

Figure 36: $\langle \Delta D \rangle$ and $\langle \Delta D_{ABS} \rangle$ (measured vs simulated) for irregularly shaped targets. The vertical bars represent the standard deviation of the mean global dose differences

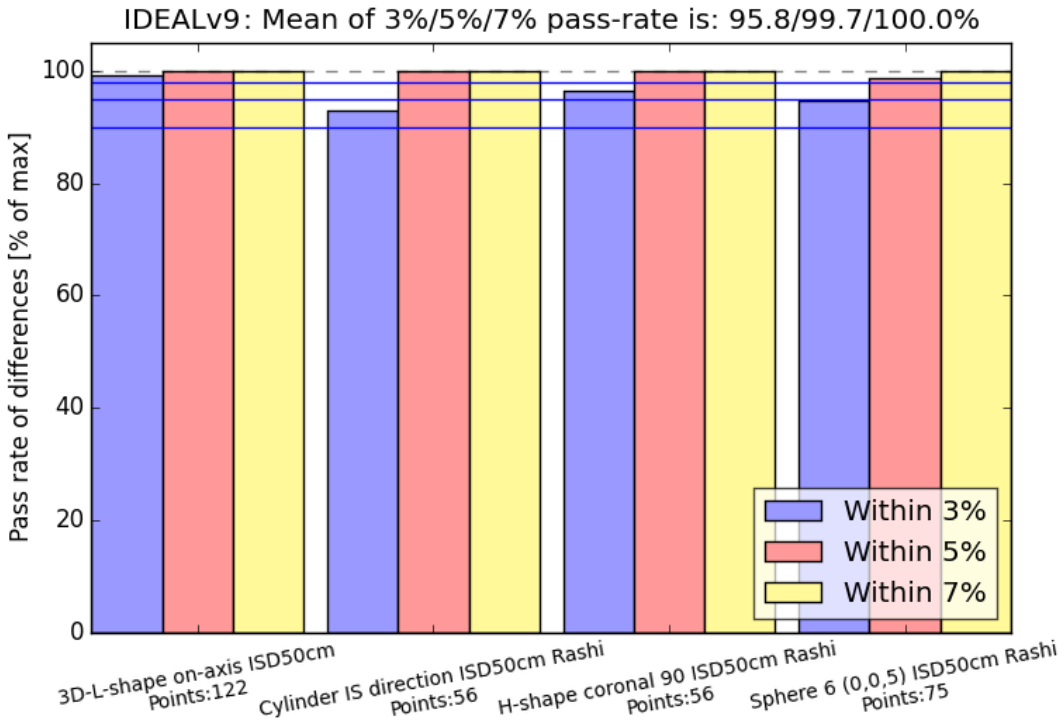

Figure 37: Percentage of PPs that agree within $3\%/5\%/7\%$ global dose difference (measured vs simulated) for cubic dose distributions. The horizontal blue lines represent $98\%/95\%/90\%$

3.3 Summary of results and discussion

The validation results of the ROS are summarized in table 3. The deviation seen in the validation is likely due to different interpolation methods used by the TPS and the ROS. All functionalities were successfully validated. The extraction of the doses was successfully validated against the already commissioned program MA_QA_v4. A first version of ROS (v1.0) for the fixed horizontal beam line was released and can be used for the commissioning of IDC software.

Isocenter to phantom surface distance [cm]	pass-rate (%)			dose deviation (%)	
	3	5	7	signed	unsigned
0	100.0	100.0	100.0	-0.1	0.1
50	99.2	100.0	100.0	0.0	0.2

Table 3: Validation results of the ROS

As for IDEALv0.9, both the cubic dose distributions and the irregularly shaped targets show good agreement with measurement (Table 4). The mean signed and unsigned dose deviations are within $\pm 2\,\%$ for all plans. Irregular targets show a slightly higher deviation. This is likely due to the fact that irregularly shaped targets contain more gradient regions. More investigations are

needed to determine whether this deviation is due to measurement uncertainties in the gradient region or due to the simulation. The results show slightly better agreement for plans without range shifter (in terms of signed dose deviation) and for plans at ISD50cm (in terms of pass-rate). This can be seen in table 5. Both of these tendencies are in line with expectations. The range shifter introduces a source of scattering in the beam path. The better agreement at ISD50cm is likely due to the reduced air gap as there are fewer scattering events.

		pass-rate(%)			dose deviation(%)	
		3	5	7	signed	unsigned
3D cubes	ISD0cm	95.8	99.3	100.0	0.4	1.0
	ISD50cm	98.0	100.0	100.0	0.5	1.0
Irregular targets	ISD0cm	93.6	97.1	98.6	0.6	1.2
	ISD50cm	96.3	99.7	99.9	0.6	1.1
3D cubes (weighted by number of PPs)	ISD0cm	97.0	99.6	100.0	0.5	1.0
	ISD50cm	98.4	100.0	100.0	0.4	0.9
Irregular targets (weighted by number of PPs)	ISD0cm	93.3	96.7	98.5	0.7	1.3
	ISD50cm	96.9	99.8	99.9	0.6	1.0

Table 4: Results of the evaluation of IDEALv0.9. Averages for 3D cubes and irregular targets for ISD0cm and ISD50cm. As there are significantly more measurements for some plans than others, the averages weighted by the number of PPs was added

	pass-rate(%)			dose deviation(%)	
	3	5	7	signed	unsigned
Average without range shifter (ISD50cm)	97.4	99.9	99.9	0.4	1.0
Average with range shifter (ISD50cm)	96.1	99.8	100.00	0.8	1.2
Average at ISD0cm	94.9	98.2	99.3	0.6	1.1
Average at ISD50cm	97.4	99.9	99.9	0.5	1.0

Table 5: Averages of plans at ISD0cm and ISD50cm as well as averages of plans with and without range shifter. Range shifters are only used clinically in combination with the reduced air gap at ISD50cm

Analyzing horizontal- and depth-dose-curves indicate a slight positional offset, which is currently under investigation. The ROS is not the best tool to determine the exact magnitude of this offset, nor is a comparison with measurement, considering that the offset is well within the uncertainty of the PP-measurements. The shift, although small, seems to be consistent with a large number of plans, which would point to a systematic offset in the IDEALv0.9 simulations.

4 Outlook

The next steps for the ROS will be on implementing a version compatible with the vertical beam line. As for IDEAL, more complex plans including oblique incidences and more heterogeneous material will be simulated and evaluated. It is also planned to generate carbon ion plans and evaluate them against measurement. There already exists a large data set of carbon measurements that has been acquired for the commissioning of carbon ion treatment, which can be reused for this purpose.

References

Benedikt, M., Gutleber, J., Dorda, U., Fabich, A., Palm, M., and Pirkl, W. (2010). Overview of the medaustron design and technology choices. (No. CERN-ATS-2010-116).

Bray, F., Ferlay, J., Soerjomataram, I., Siegel, R. L., Torre, L. A., and Jemal, A. (2018). Global cancer statistics 2018: Globocan estimates of incidence and mortality worldwide for 36 cancers in 185 countries. *CA: a cancer journal for clinicians*, 68(6):394–424.

Carlino, A. (2017). Implementation of advanced methodologies in the commissioning of a light ion beam therapy facility.

Carlino, A. (2018a). MP QA Operating Procedure Document: Dosimetrical patient specific plan verification for IR2 with protons. MedAustron report.

Carlino, A. (2018b). TPS RayStatioin 5.0: Dosimetric Commissioning report, proton planning IR3. MedAustron report.

Elia, A. (2019). *Characterization of the GATE Monte Carlo platform for non-isocentric treatments and patient specific treatment plan verification at MedAustron-Vienna-Austria*. PhD thesis.

Grevillot, L. (2011). *Monte Carlo simulation of active scanning proton therapy system with Gate/Geant4: Towards a better patient dose quality assurance*. PhD thesis, Lyon, INSA.

Grevillot, L. (2019). Monte Carlo simulation in scanned ion beam therapy, A medical physicist perspective. Presented at OMA Advanced School on Medical Accelerators and Particle Therapy. Retrieved March 28, 2020, from https://indico.cern.ch/event/775870/contributions/3228301/attachments/1824890/2986189/LGR-OMA2019_MC-FINAL_Shared.pdf.

Grevillot, L., Osorio Moreno, J., Letellier, V., Dreindl, R., Elia, A., Fuchs, H., Carlino, A., Kragl, G., Palmans, H., Vatnitsky, S., et al. (2019). Clinical implementation and commissioning of the medaustron particle therapy accelerator for non-isocentric scanned proton beam treatments. *Medical physics*.

IAEA (2008). *Relative biological effectiveness in ion beam therapy*. International Atomic Energy Agency.

ICRU (2016). ICRU REPORT No. 93, PRESCRIBING, RECORDING, AND REPORTING LIGHT ION BEAM THERAPY. *Journal of the ICRU*, 16(1-2).

Jägerhofer, L. and Wurzer, P. (2017). Medaustron–a new austrian synchrotron facility for cancer therapy and research.

Jan, S., Benoit, D., Becheva, E., Carlier, T., Cassol, F., Descourt, P., Frisson, T., Grevillot, L., Guigues, L., Maigne, L., et al. (2011). Gate v6: a major enhancement of the gate simulation platform enabling modelling of ct and radiotherapy. *Physics in Medicine & Biology*, 56(4):881.

Levin, W., Kooy, H., Loeffler, J., and DeLaney, T. (2005). Proton beam therapy. *British journal of Cancer*, 93(8):849–854.

Matysiak, W., Yeung, D., Slopsema, R., and Li, Z. (2016). Evaluation of the range shifter model for proton pencil-beam scanning for the Eclipse v. 11 treatment planning system. *Journal of applied clinical medical physics*, 17(2):391–404.

Newhauser, W., Fontenot, J., Zheng, Y., Polf, J., Titt, U., Koch, N., Zhang, X., and Mohan, R. (2007). Monte carlo simulations for configuring and testing an analytical proton dose-calculation algorithm. *Physics in Medicine & Biology*, 52(15):4569.

Newhauser, W. D. and Zhang, R. (2015). The physics of proton therapy. *Physics in Medicine & Biology*, 60(8):R155.

Osmić, F., Koschik, A., Urschütz, P., and Benedikt, M. (2014). Status of medaustron–the austrian ion therapy and research centre.

Paganetti, H. (2002). Nuclear interactions in proton therapy: dose and relative biological effect distributions originating from primary and secondary particles. *Physics in Medicine & Biology*, 47(5):747.

Paganetti, H. (2012). Range uncertainties in proton therapy and the role of monte carlo simulations. *Physics in Medicine & Biology*, 57(11):R99.

Paganetti, H., Jiang, H., Parodi, K., Slopsema, R., and Engelsman, M. (2008). Clinical implementation of full Monte Carlo dose calculation in proton beam therapy. *Physics in Medicine & Biology*, 53(17):4825.

PTW (2019/2020). *DETECTORS, including Codes of Practice*. Detectors catalog.

Saini, J., Maes, D., Egan, A., Bowen, S. R., St James, S., Janson, M., Wong, T., and Bloch, C. (2017). Dosimetric evaluation of a commercial proton spot scanning monte-carlo dose algorithm: comparisons against measurements and simulations. *Physics in Medicine & Biology*, 62(19):7659.

Sánchez Parcerisa, D. (2012). *Experimental and computational investigation of water-to-air stopping power ratio for ion chamber dosimetry in carbon ion radiotherapy*. PhD thesis.

Sawakuchi, G. O., Titt, U., Mirkovic, D., Ciangaru, G., Zhu, X. R., Sahoo, N., Gillin, M. T., and Mohan, R. (2010). Monte carlo investigation of the low-dose envelope from scanned proton pencil beams. *Physics in Medicine & Biology*, 55(3):711.

Sawakuchi, G. O., Titt, U., Mirkovic, D., and Mohan, R. (2008). Density heterogeneities and the influence of multiple coulomb and nuclear scatterings on the bragg peak distal edge of proton therapy beams. *Physics in Medicine & Biology*, 53(17):4605.

Schreiner, T., Stock, M., Georg, P., and Georg, D. (2019). Medaustron: First years of operation. *Nuclear Physics News*, 29(2):22–24.

Seco, J. and Verhaegen, F. (2013). *Monte Carlo techniques in radiation therapy*. CRC/Taylor & Francis.

Soukup, M., Fippel, M., and Alber, M. (2005). A pencil beam algorithm for intensity modulated proton therapy derived from monte carlo simulations. *Physics in Medicine & Biology*, 50(21):5089.

Stock, M., Georg, P., Mayer, R., Böhlen, T. T., and Vatnitsky, S. (2015). Development of clinical programs for carbon ion beam therapy at medaustron. *International journal of particle therapy*, 2(3):474–477.

Tobias, C., Lawrence, J., Born, J., McCombs, R., Roberts, J., Anger, H., Low-Beer, B., and Huggins, C. (1958). Pituitary irradiation with high-energy proton beams a preliminary report. *Cancer research*, 18(2):121–134.

Wilson, R. R. (1946). Radiological use of fast protons. *Radiology*, 47(5):487–491.